6 Small-Scale Processes

Miles G. McPhee
McPhee Research Company
Naches, Washington

I. Introduction

The direct interaction between polar oceans and the atmosphere occurs across a relatively thin boundary layer, which differs from the upper part of the rest of the world ocean in that its properties and physics are affected directly by a layer of ice which may reach several meters in thickness. The small-scale oceanic processes which affect air–sea–ice interaction in polar

Polar Oceanography, Part A: Physical Science

regions are the subject of this chapter. The main thrust is describing the physical processes that control the exchange of heat, mass, and momentum near the surface when sea ice is present. The problems addressed, which are pertinent in most respects to all upper-ocean physics, tax the best observational and theoretical tools we have. Oceanographic measurements in polar oceans are expensive and often difficult. Remote sensing is hampered by long polar nights and persistent cloudiness. Quantitative theoretical treatment requires a thorough understanding of turbulent boundary layer dynamics, influenced by rotation, buoyancy, and sea ice. Despite the difficulties, there has been heightened interest and much progress in recent years, driven by both increased operational needs and recognition of the role that polar and subpolar oceans play in long-term climate fluctuations, especially ventilation of the deep ocean.

The story begins nearly a century ago with F. Nansen and the drift of the research vessel *Fram* in the ice pack of the Eurasian basin of the Arctic Ocean. Nansen observed that the ice consistently veered 20° to 40° to the right of the surface wind. He correctly surmised that the veering resulted from the Coriolis force (i.e., the apparent deflection of an object moving in a rotating reference frame) acting differentially at various levels in the shear flow beneath the ice. Nansen interested V. Ekman in the problem, and in a remarkable paper published in 1905, Ekman developed the mathematics of a sheared fluid on a rotating surface, discovering elegantly simple spirals in theoretical profiles of mean current and turbulent stress. His theory predicted that surface current should be 45° to the right *(cum sole)* of surface stress, which explained qualitatively Nansen's observations. He also showed how large, circular motions superimposed on the mean drift (inertial oscillations) could develop in the upper ocean and further suggested that the eddy viscosity relating current shear to turbulent stress depended on surface stress. In the last two areas, Ekman was far ahead of his time, and it was not until the latter half of the century that observations (and, in some respects, theory) caught up with him.

Ekman's paradigm failed to account for a thin region near the ice/ocean interface where strong shear develops parallel to the direction of interfacial stress. By considering data from Soviet Polar Drift stations, Shuleikin (1938) patched the ice to the Ekman solution via a thin surface layer and worked out the intricate force balance that determines ice response to wind in the absence of internal stress gradients. Reed and Campbell (1962) later incorporated these concepts into their ice modeling work, modifying them somewhat by letting the eddy viscosity of the lower, Ekman layer depend on the interfacial stress.

Strong inferential evidence for Ekman dynamics was found in the rightward (leftward in the southern hemisphere) deflection of ice drift and surface currents, but there was no unequivocal example of an Ekman spiral in

upper-ocean currents until Hunkins (1966) presented measurements made from Arctic Drift Station Alpha during the summer of 1958 (Fig. 6.1). Hunkins interpreted his measurements as including three more or less separate currents: (1) a geostrophic current, $\mathbf{V}_g$, associated with slope of the sea surface and not dependent on the recent, local wind; (2) the Ekman spiral up through the boundary layer, culminating in $\mathbf{V}_0$; and (3) a thin (less than 2 m) layer of intense shear, indicated by the relative velocity, $\mathbf{V}_2$. These three elements are present in nearly all current measurements made from drifting ice, provided the currents are averaged long enough that inertial effects are not dominant.

During the 1960s and 1970s, advancing technology and increased interest in high-latitude oceanography led to greater understanding of ice/ocean interaction. This was accompanied by a gradual shift in attitude from treating the ice as a barrier preventing oceanic access to appreciating its potential as an amazingly stable platform for conducting high-resolution experiments

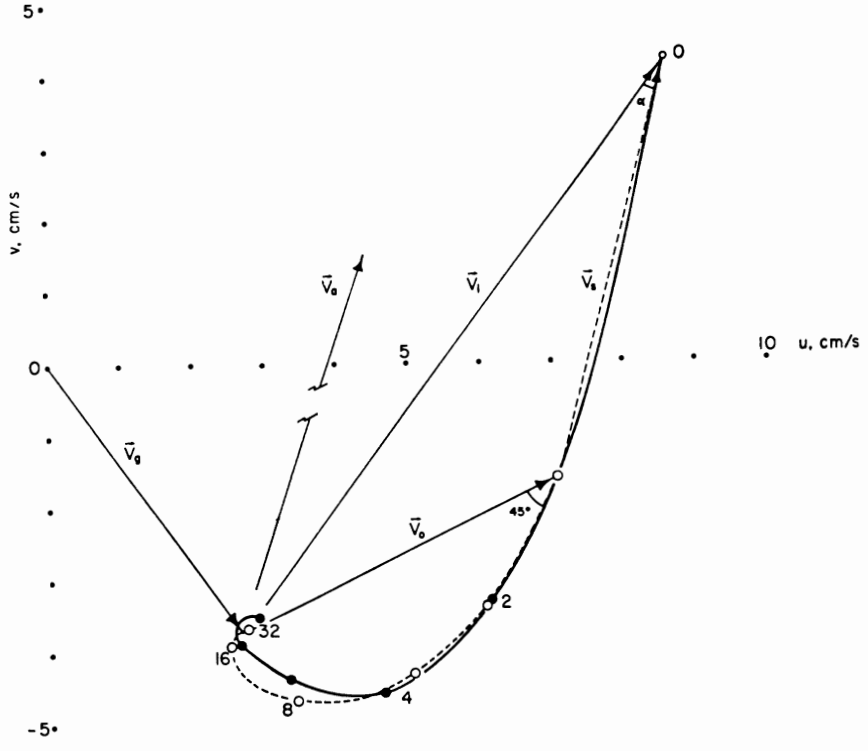

Figure 6.1 Vector average of nine current profiles taken over a 2-month period at drift station Alpha (filled circles), shown with Ekman current spiral for eddy viscosity of 23.8 $cm^2 s^{-1}$ (open circles). Reprinted with permission from Hunkins (1966); copyright by Pergamon Press.

in the boundary layer and pycnocline. Neshyba *et al.* (1971) reported, in unprecedented detail, small-scale step structure in the thermocline under drifting ice island T-3. Pilot studies of the Arctic Ice Dynamics Joint Experiment (AIDJEX) in 1971 and 1972 included the elegant turbulence experiments of Smith (Smith, 1974; McPhee and Smith, 1976). The year-long AIDJEX Main Experiment (1975–1976) provided unsurpassed time series of upper-ocean currents and temperature/salinity profiles at multiple stations in the central Arctic (Hunkins, 1980). At the same time, rapid advances in atmospheric planetary boundary layer theory, aided by computer modeling, were providing a broader context for interpreting the measurements.

After AIDJEX, emphasis shifted toward the complicated interactions that occur near the lateral boundaries of the sea ice, i.e., the marginal ice zone (MIZ). Large, multidisciplinary experiments such as MIZEX West in the Bering Sea and the series of MIZEX East experiments in the Greenland Sea MIZ examined the interplay between thermodynamics and dynamics as the ice encounters relatively warm water. Interest in high Arctic upper-ocean processes, especially the internal wave climate, has revived, as witnessed by the Arctic Internal Wave Experiment (AIWEX 85) and the planned Co-ordinated Eastern Arctic Experiment (CEAREX) operations in the eastern Arctic. These projects have spawned significant improvements in measurement technology, including sophisticated velocity/temperature/conductivity profilers (Morison *et al.*, 1987; Villanueva and van Leer, 1987), acoustic Doppler profilers (Pinkel *et al.*, 1986), and direct turbulent heat flux measurements (McPhee, 1986a). A recent transect of the mixed layer in the Weddell Sea (Gordon, 1987) has revealed fascinating contrasts with the relatively well-documented Arctic mixed layer that call out for further study.

It would be difficult to summarize adequately all of this work, even the most recent, in a short chapter. The intent is rather to provide the reader with a general view of our current understanding of small-scale processes near the ice/ocean interface. As such, the chapter necessarily reflects some of my personal views, which a properly skeptical reader will recognize. In some cases (specifically, Section III,C), what I call "simple" might justifiably be called anything but; however, the description is related to alternatives, mainly numerical modeling, and I have tried to identify the underlying concepts, which, in the main, are quite simple.

II. Fundamental Physics

This section presents a brief synopsis of the fundamental fluid equations pertinent to understanding upper-ocean transfer processes. For a reader not familiar with the fluid equations or elementary vector and tensor notation, a

number of standard textbooks treat the concepts well. Gill (1982, Chapters 3 and 4) presents an especially clear and useful development of the state equations, conservation equations, and equation of motion.

A. Conservation Equations

The equations that govern fluid behavior may be stated in relatively compact form. Let ϵ be an arbitrary property of the fluid, say density, internal energy (or equivalently in our case, heat content), or concentration of salt or some other contaminant such as frazil ice crystals, or a vector quantity such as momentum. Consider a fixed, infinitesimal control volume in the fluid. Within the volume, the local rate of change of ϵ will depend on a source of the property, Q_ϵ, less the net flux, $\mathbf{F}_\epsilon$, integrated over the surface of the control volume. By Gauss's theorem

$$\partial\epsilon/\partial t = Q_\epsilon - \nabla \cdot \mathbf{F}_\epsilon \tag{6.1}$$

For scalars, the source term Q_ϵ is associated mainly with phase changes; e.g., if frazil crystals form in supercooled water, heat and salt are released locally, so local internal energy and salinity increase. In most situations, the source term for scalars will be small.

The flux vector (or tensor when ϵ is momentum) $\mathbf{F}_\epsilon$ may comprise several elements, examples being the advective flux $\epsilon\mathbf{u}$, where $\mathbf{u}$ is the local velocity vector; a molecular diffusion term $-\rho k_\epsilon \nabla\epsilon$, where k_ϵ is the molecular diffusivity coefficient; or, when ϵ is internal energy, a radiative flux associated with insolation. By far the most important element for the rotational boundary layer (RBL) is the advective term, so as a first approximation the flux vector may be written

$$\mathbf{F}_\epsilon \cong \epsilon\mathbf{u} \tag{6.2}$$

but note that there may be special circumstances where other terms are important, pertinent examples being solar heating when ice concentration is low (radiative flux divergence) and molecular viscosity effects in a thin layer near the ice/ocean interface.

For dynamical purposes, most oceanic flows may be treated as incompressible, meaning that density ρ following fluid parcels does not change (i.e., the material derivative is zero). This leads directly to the continuity equation

$$\nabla \cdot \mathbf{u} = -(1/\rho)\,(d\rho/dt) = 0 \tag{6.3}$$

If Eq. (6.2) (advective flux) and Eq. (6.3) (continuity) are incorporated into Eq. (6.1), the general conservation equation may be written

$$\partial\epsilon/\partial t + \mathbf{u} \cdot \nabla\epsilon = Q_\epsilon \tag{6.4}$$

Substituting salinity ρS for ϵ, the conservation of salt is expressed as

$$\partial S/\partial t + \mathbf{u} \cdot \nabla S = Q_S/\rho \tag{6.5}$$

where Q_S is a salinity source within the fluid (e.g., from nucleation of frazil crystals).

Provided divergence of radiative flux is incorporated into a source term Q_h, which may also include latent heat associated with phase change, we can write a similar equation for temperature:

$$\partial T/\partial t + \mathbf{u} \cdot \nabla T = Q_h/\rho c_p \tag{6.6}$$

where c_p is the specific heat at constant pressure. Specific heat varies with temperature, salinity, and pressure (see Gill, 1982, Table A3.1); however, the variation is relatively small, and here we use a constant value of 3980 J kg^{-1} K^{-1}.

Now substitute vector momentum $\rho\mathbf{u}$ for ϵ in Eq. (6.4). We have

$$\partial \mathbf{u}/\partial t + \mathbf{u} \cdot \nabla \mathbf{u} = Q_f/\rho \tag{6.7}$$

In this interpretation, the source term is the vector sum of the negative gradient of pressure in the fluid, $-\nabla p$, and gravity, $-g\mathbf{k}$, where $\mathbf{k}$ is the vertical unit vector. Thus we arrive at Euler's equation

$$\partial \mathbf{u}/\partial t + \mathbf{u} \cdot \nabla \mathbf{u} = -(1/\rho)\,\nabla p - g\mathbf{k} \tag{6.8}$$

This is, of course, a highly simplified derivation of Newton's second law for fluids. Batchelor (1970, Chapter 3) treats the subject in detail.

B. Reynolds Stress

Ignoring molecular effects in the conservation equations is not the same as assuming that the fluid is frictionless. When ice moves in response to wind, it encounters drag from the water, which indicates a net downward momentum flux. Unless the forcing is very small, we know that in the bulk of the RBL molecular transfer processes can account for only a minute fraction of the total momentum flux. The remainder occurs in a way that can best be shown by manipulating the advective term in the momentum equation. Suppose that the flow velocity consists of rapid variations superimposed on an underlying "mean" signal that changes relatively slowly in response to the large-scale forcing. Over some area large compared with the scale of the small, frequent fluctuations, we may express the local instantaneous flow as

$$\mathbf{u} = \langle \mathbf{u} \rangle + \mathbf{u}' \tag{6.9}$$

where the angle brackets indicate the mean over the area and $\mathbf{u}'$ is the

deviation from the mean ($\langle \mathbf{u}' \rangle = 0$). With the continuity condition, Eq. (6.3), and the well-known rule for the average of products,

$$\langle u_i u_j \rangle = \langle u_i \rangle \langle u_j \rangle + \langle u_i' u_j' \rangle \tag{6.10}$$

the average of the advective term [the second term on the left of Eq. (6.8)] can be expressed in component form as

$$\langle u_i \frac{\partial u_j}{\partial x_i} \mathbf{e}_j \rangle = \left(\langle u_i \rangle \frac{\partial \langle u_j \rangle}{\partial x_i} + \frac{\partial \langle u_i' u_j' \rangle}{\partial x_i} \right) \mathbf{e}_j \tag{6.11}$$

where $\mathbf{e}_j$ is the unit vector in the j direction ($j = 1, 2, 3$; repeated indices imply summation; and by convention $\mathbf{e}_3$ is the vertical unit vector $\mathbf{k}$).

Unless otherwise noted, from here on $\mathbf{u}$ written without angle brackets represents the underlying mean flow velocity. The Euler equation becomes

$$\partial \mathbf{u}/\partial t + \mathbf{u} \cdot \nabla \mathbf{u} = -(1/\rho) \nabla p - g\mathbf{k} + \nabla \cdot \boldsymbol{\tau} \tag{6.12}$$

where the components of the symmetric tensor $\boldsymbol{\tau}$ are

$$\tau_{ij} = -\langle u_i' u_j' \rangle \tag{6.13}$$

which is the kinematic Reynolds stress. Reynolds stress is most often associated with more or less chaotic deviations called turbulence, but internal waves (which are not in general turbulent) can also transport momentum by correlation of velocity deviations.

If ϵ is a scalar property, we may similarly write the general scalar conservation equation [Eq. (6.4)] as

$$\partial \epsilon/\partial t + \mathbf{u} \cdot \nabla \epsilon = Q_\epsilon - \nabla \cdot \langle \epsilon' \mathbf{u}' \rangle \tag{6.14}$$

where unprimed quantities again refer to underlying mean values.

C. Rotation and Geostrophy

The acceleration of a fluid parcel moving with velocity $\mathbf{u}$ relative to a frame of reference that is rotating about some axis with angular velocity $\boldsymbol{\Omega}$ includes two terms that are not present in an inertial reference frame. One of these is a centripetal acceleration, which is usually incorporated into the apparent gravity g. The other term is the Coriolis acceleration $2\,\boldsymbol{\Omega} \times \mathbf{u}$ and is often of central importance in geophysical flows. A special symbol f (the Coriolis parameter) denotes twice the vertical component of rotation,

$$f = 2\Omega_3 = 2\Omega \sin \Phi \tag{6.15}$$

where Φ is the latitude (north positive) and Ω the angular rotation speed of the earth, $7.292 \times 10^{-5}\ \mathrm{s}^{-1}$.

If we ignore the vertical component of the Coriolis term, the Euler equation in a fixed-to-earth (rotating) frame is

$$d\mathbf{u}/dt + f\mathbf{k} \times \mathbf{u} = -(1/\rho)\,\nabla p - g\mathbf{k} + \nabla \cdot \boldsymbol{\tau} \tag{6.16}$$

The *geostrophic current* is defined by

$$f\mathbf{k} \times \mathbf{u}_g \equiv -(1/\rho)\,\nabla p \tag{6.17}$$

Neglecting variation in air pressure, the surface geostrophic flow can be expressed in terms of the gradient of sea surface elevation η,

$$f\mathbf{k} \times \mathbf{u}_g = -g\,\nabla\eta \tag{6.18}$$

From Eq. (6.16), the geostrophic flow coincides with the actual flow only in a steady state with no advective flux or Reynolds stress. It is often convenient to consider flow relative to the surface geostrophic flow, e.g., wind-driven currents with respect to a relatively slowly changing geostrophic flow. With the approximation that the material derivative of $\mathbf{u}_g$ is zero, we may write Eq. (6.16) as

$$d\mathbf{u}_r/dt + f\mathbf{k} \times \mathbf{u}_r = \nabla \cdot \boldsymbol{\tau} \tag{6.19}$$

where $\mathbf{u}_r = \mathbf{u} - \mathbf{u}_g$.

Equation (6.19) provides a simple relation between kinematic stress at the surface (or ice/ocean interface) and net volume transport relative to the underlying geostrophic flow. Since our primary concern is mean horizontal current, it is convenient to express two-dimensional (horizontal) vectors as complex numbers, that is, $\hat{u} = u + iv$, where u and v are velocity components in the x and y directions and $i = \sqrt{-1}$. This has the advantage of simplifying notation and calculation (using straightforward complex arithmetic) and will be used extensively in the following sections. When a normally complex quantity $\hat{A}$ is written without the caret, scalar magnitude is implied, that is, $\hat{A} = Ae^{i\theta}$, where θ is the counterclockwise angle from the real axis, $\theta = \tan^{-1}\mathrm{Im}(\hat{A})/\mathrm{Re}(\hat{A})$. Note that complex multiplication and division implies both scaling and rotation

$$\begin{aligned} \hat{A}\hat{B} &= AB\,e^{i(\theta_A+\theta_B)} \\ \hat{A}/\hat{B} &= (A/B)e^{i(\theta_A-\theta_B)} \end{aligned} \tag{6.20}$$

For a horizontally homogeneous system (i.e., no horizontal gradients), Eq. (6.19) becomes in complex notation

$$d\hat{u}_r/dt + if\hat{u}_r = \partial\hat{\tau}/\partial z \tag{6.21}$$

where $\hat{\tau}$ is the horizontal traction vector component of the Reynolds stress tensor,

$$\hat{\tau} = -(\langle u'w' \rangle + i\langle v'w' \rangle) \tag{6.22}$$

We suppose that at some level the Reynolds stress driven by surface momentum flux decreases to zero, so integrating Eq. (6.21) from the maximum depth of frictional influence, H, we have

$$\frac{d\hat{M}}{dt} + if\hat{M} = \hat{\tau}(z=0) = \hat{\tau}_0$$
$$\hat{M} = \int_{-H}^{0} \hat{u}_r \, dz \tag{6.23}$$

This equation allows a steady-state balance in which the integrated transport is equal to the surface stress divided by f, directed 90° *cum sole* (clockwise in the northern hemisphere) to the stress direction.

Suppose a system obeying Eq. (6.23), initially at rest, is subjected to a step-function wind stress in the imaginary (y) direction, $\hat{\tau} = i\tau$, at $t = 0$. The solution for $t > 0$ is

$$\hat{M}(t) = \frac{\tau}{f}(1 - e^{-ift}) = \frac{\tau}{f}[1 - \cos(ft) + i\sin(ft)] \tag{6.24}$$

The locus of solutions of Eq. (6.24) in the complex plane is a circle of radius τ/f centered at τ/f on the real axis; thus the transport vector traces a clockwise circle about its mean value in one inertial period, $2\pi/f$, which is 12 h at the pole. A trajectory traced out by the mean transport shows a series of cycloidal scallops, called inertial oscillations. This may seem highly idealized, but in fact we often find large circular motions superimposed on a relatively small mean translation in ice drift trajectories (e.g., Hunkins, 1967; McPhee, 1978), which persist for up to 8 or 10 inertial periods and are clearly related to abrupt changes in wind forcing.

D. Fluid Properties

Density of seawater depends on pressure, temperature, and dissolved salts, indicated by practical salinity S. Formulas for calculating density from T, p, and S are given by Gill (1982, Appendix 3), along with tables for quick reference.

It is often relative changes in density that are important dynamically, and then it is convenient to relate the changes directly to changes in temperature and salinity via expansion coefficients:

$$\Delta\rho/\rho = -\beta_T \Delta T + \beta_S \Delta S \tag{6.25}$$

β_S has a weak dependence on temperature but for polar waters can be approximated by the constant value 0.81×10^{-3} (Gill, 1982; Table A3.1). β_T varies with both temperature and salinity (see, e.g., Table 3.1 of Neumann and Pierson, 1966). Two points are worth noting. First, for salinities above

about 25 ppt, the thermal expansion coefficient is positive for all temperatures above freezing. Thus seawater does not exhibit a density maximum like that found at about 4°C in fresh water. Second, at temperatures near freezing, β_T is about an order of magnitude smaller than at moderate (15°C) temperatures, so that at low temperatures the density is controlled mainly by changes in salinity.

The UNESCO formula for the freezing temperature of saline water in degrees Celsius is given by Gill (1982):

$$T_f(S, p) = -0.0575S + 1.710523 \times 10^{-3} S^{3/2} - 2.154996 \times 10^{-4} S^2 - 7.73 \times 10^{-3} p \qquad (6.26)$$

where S is salinity in parts per thousand and p is pressure in bars. A straight-line fit to Eq. (6.26) yields $T_f = -0.054S$ at surface pressure. Note that the freezing point is depressed by about 0.008° for every 10-m increase in depth. Thus water which is at its *in situ* freezing temperature at depth will be supercooled if brought to higher levels.

III. Turbulent Exchange: Processes and Scales

In this section, a relatively simple conceptual view of turbulence in the under-ice RBL is constructed, using the fundamentals of Section II along with basic scaling principles. We review the mixing-length hypothesis, discuss what controls the scales of the turbulence, and relate the concepts in a heuristic model of turbulent exchange.

A. Turbulence

When inertial forces in a fluid become large compared with viscous forces (i.e., as the Reynolds number increases), the fluid behavior becomes highly nonlinear (chaotic) and a deterministic description of turbulent flow is virtually impossible. We resort instead to characterizing the statistics of the turbulent flow and seek to relate turbulent fluxes implicit in the statistics to mean flow quantities. Much research and an extensive literature exist on turbulence in rotating planetary boundary layers (see, e.g., Friehe, 1987; Price *et al.*, 1987; Wyngaard, 1985; Mellor and Yamada, 1982), although, with the exception of the atmospheric surface layer, data are still relatively sparse. Characteristics of turbulence in the ice/ocean boundary layer are described by McPhee and Smith (1976) and reviewed by McPhee (1986b). Although the general topic and its various theoretical underpinnings are far too vast to attempt to summarize here, there are some surprisingly simple ideas that explain much (but certainly not all!) about the behavior of the ice/ocean RBL, even in relatively complex situations like the marginal ice

zone. The intent of this section is not to present a comprehensive review but rather to equip the reader with some useful tools for treating small-scale processes.

There is no generally accepted definition of turbulence, but Tennekes and Lumley (1972) list several characteristics of a turbulent flow which identify it as such: (1) turbulence is irregular and seemingly random; (2) it is highly diffusive; (3) it is always highly rotational; and (4) it is essentially dissipative, meaning that the energy transfer in turbulence is always toward increasing internal energy (and entropy) of the fluid at the expense of the flow's overall kinetic or potential energy. Turbulence accomplishes diffusion much more efficiently than is possible by molecular processes alone. Ultimately, energy is dissipated at molecular scales by molecular processes; the main impact of turbulence is to involve many more molecules.

Picture a turbulent disturbance centered at some level in a flow with a positive vertical gradient of some arbitrary property ϵ. As it overturns, the eddy (which is highly diffusive) will distribute an excess of ϵ below the plane and a deficit above. The net result is a downward flux of ϵ. The mixing-length hypothesis (see, e.g., Hinze, 1975, Chapter 5) is simply that this flux should depend on three quantities: (1) the gradient of ϵ; (2) a velocity scale u_ϵ proportional to the eddy velocity in the direction of the gradient; and (3) a length scale λ characteristic of the distance over which the most energetic eddies transport the fluid, such that the smaller eddies can "keep up" in diffusing away deviations of ϵ from the local ambient value. The simplest expression for vertical flux is

$$F_\epsilon = -ku_\epsilon \lambda \, \partial\epsilon/\partial z \tag{6.27}$$

where k is von Karman's constant, equal to 0.4.

By analogy with molecular diffusivity (which is proportional in an ideal gas to the product of the root-mean-square velocity of the molecules and their mean free path) we may define an "eddy diffusivity"

$$K_\epsilon = ku_\epsilon \lambda \tag{6.28}$$

From Section II,B, when a flow with rapid fluctuations about some mean value is averaged in an ensemble sense, Reynolds flux terms appear in the conservation equations. Equation (6.27) provides a link between the turbulent Reynolds fluxes and the mean flow properties. Our main concern is vertical flux, and we have for temperature, salinity, and horizontal momentum:

$$\langle w'T' \rangle = -K_T \, \partial T/\partial z \tag{6.29}$$

$$\langle w'S' \rangle = -K_S \, \partial S/\partial z \tag{6.30}$$

$$\hat{\tau} = -(\langle u'w' \rangle + i\langle v'w' \rangle) = K_m \, \partial\hat{u}/\partial z \tag{6.31}$$

In the context of the mixing-length hypothesis, the different eddy diffusivities imply different length scales; e.g., under certain circumstances, momentum is "diffused" much more effectively (by pressure terms in the covariance equations) than is a scalar like salt, which requires direct diffusion at the molecular level. However, in the absence of density gradients and far enough from solid boundaries, we expect the eddy diffusivities to be roughly equivalent. In such cases, the "Reynolds analogy" is often invoked, which treats all the eddy diffusivities as equal.

The mixing-length hypothesis is only one way of addressing the "closure" problem of turbulence, i.e., relating the Reynolds flux terms to mean flow properties. Another is "second-order" closure, in which ensemble-averaged equations for the covariance equations are solved simultaneously with the mean equations. A useful strategy is to solve numerically the full set of equations, closed at second order, and then use the solutions to derive much simpler equations for closure at the mean (first-order) level. Mellor and Yamada (1982) describe a hierarchy of closure schemes, developed within one basic theoretical framework, that has been used successfully to model many different types of turbulent flow, including the under-ice RBL (Mellor *et al.*, 1986).

A different approach is the so-called large-eddy-simulation (LES) model, which solves the time-dependent, three-dimensional equations for grid scales small enough (within the inertial subrange of the turbulence spectrum) to resolve the large, energy-containing eddies explicitly (e.g., Deardorff, 1972; Moeng, 1984). To learn about the ensemble statistics of the large eddies, LES model output is essentially treated as a substitute for actual measurements. The computing power required for LES models is formidable, but as supercomputers become more accessible, LES models may provide useful answers for some difficult problems, e.g., how drag is affected by various scales of under-ice topographic relief.

B. Scales Governing RBL Turbulence

Certain scaling principles seem to describe turbulent mixing in the ice–ocean RBL reasonably well. The first is that the local turbulent velocity scale u_ϵ in Eq. (6.27) is proportional to the square root of the horizontal turbulent shear stress. Here we define the *friction velocity* scale as a vector rather than a scalar.

$$\hat{u}_* = \frac{\hat{\tau}}{\sqrt{\tau}} = -\frac{(\langle u'w' \rangle + i\langle v'w' \rangle)}{(\langle u'w' \rangle^2 + \langle v'w' \rangle^2)^{1/4}} \tag{6.32}$$

The friction velocity at the ice/ocean interface is

$$\hat{u}_{*0} = \hat{\tau}_0/\sqrt{\tau_0} \tag{6.33}$$

In the RBL, stress decreases from its surface value to zero at depth; thus an obvious scale for kinematic stress is $u_{*0}\hat{u}_{*0}$.

The length scale for vertical exchange depends on several factors, and describing it correctly is the crux of the mixing-length problem. In a steady, horizontally homogeneous RBL the scale is governed in varying degrees by the distance from the surface, the "planetary" length, u_*/f and the Obukhov length associated with gravitational effects on turbulent overturn.

For a neutrally stratified turbulent flow in the vicinity of the "wall," i.e., the ice/ocean or air/ocean interface, the length scale depends on the distance from the wall

$$\lambda = |z| \qquad \text{(surface layer)} \tag{6.34}$$

Much is known about this flow regime (see, e.g., Hinze, 1975, Chapter 7), which includes the lower tens of meters of the atmospheric boundary layer and most turbulent flows important in engineering problems. Variation in turbulent stress across the region of validity of Eq. (6.34) is small, and it is often a fairly good approximation to set $u_* = \text{constant} = u_{*0}$, which results in the "law of the wall"

$$\frac{\hat{u}}{\hat{u}_{*0}} = \frac{1}{k}\ln|z| + C = \frac{1}{k}\ln\frac{|z|}{z_0} \tag{6.35}$$

where $C\,[= -\ln(z_0)/k]$ is an integration constant; z_0 is called the *roughness length;* and $\hat{u}$ is the velocity relative to the interface, which varies logarithmically with distance from the interface in the direction of stress. Equation (6.35) is valid only in the region where the mixing length varies with z and where stress is nearly constant. The region is commonly called the *surface layer* and comprises roughly one-tenth of the entire RBL depth.

As the distance from the interface increases, the scale of the eddies does not continue to grow without bound. In the outer, "free-turbulence" region beyond the surface layer, we find from both measurements and dimensional analysis (see also the stability analysis arguments of Stern, 1975, Chapter 8) that the turbulent length scale for the neutral RBL is approximately

$$\lambda_N = \xi_N u_*/f \qquad \text{(outer layer)} \tag{6.36}$$

where ξ_N is a constant, approximately equal to 0.05 (McPhee, 1981). If the eddy scale increases linearly near the interface, the extent of the surface layer is of order $\xi_N u_{*0}/f$.

The third major factor affecting the length scale of turbulence in the RBL is buoyancy, i.e., the gravitational force that tends to retard (or enhance, if unstable) vertical motion when a density gradient is present. When variations in density are small relative to mean density, as is the case in the RBL, the small fluctuations are important dynamically only when they occur in

combination with gravity (the Boussinesq approximation). It is then convenient to define a buoyancy flux

$$\langle b'w' \rangle = (g/\rho) \langle \rho'w' \rangle \tag{6.37}$$

where $\langle \rho'w' \rangle$ is the Reynolds mass flux. [Although it violates the literal sense of the word, the convention adopted here is that buoyancy flux and turbulent mass flux are in the same direction; many authors prefer a minus sign in Eq. (6.37).]

There are two main sources of buoyancy flux in the ice-covered RBL: melting or freezing at the ice/ocean interface and turbulent entrainment at the mixed-layer/pycnocline interface. The buoyancy flux may be expressed in terms of (kinematic) heat and salt flux using Eq. (6.25):

$$\langle b'w' \rangle = g(\beta_S \langle w'S' \rangle - \beta_T \langle w'T' \rangle) \tag{6.38}$$

Because of the disparity in expansion coefficients at low temperatures, buoyancy flux in polar waters is controlled mainly by salinity, even though the thermodynamic forcing is usually heat flux associated with temperature gradients. The reason for this is that sea ice excludes all but a small fraction of the salt in seawater as it freezes; hence freezing is associated with downward buoyancy flux and melting with upward buoyancy flux, even though the buoyancy due to heat flux is in the opposite sense.

Obukhov (1946, see English translation, 1971) examined the effect of buoyancy on surface layer dynamics by considering the turbulent kinetic energy budget (see, e.g., Tennekes and Lumley, 1972); however, a simpler heuristic argument adapted from Businger and Arya (1974) serves our purpose here. Consider again an overturning eddy in a density gradient. A parcel of fluid with vertical velocity w' will convert its kinetic energy to potential energy after it has traveled a vertical distance λ when

$$-g\delta\rho\lambda \cong -g\frac{\partial \rho}{\partial z}\lambda^2 \propto \rho\langle w'^2 \rangle \propto \rho u_*^2 \tag{6.39}$$

Since

$$\partial\rho/\partial z = -\langle \rho'w' \rangle / K = -\langle \rho'w' \rangle / k\lambda u_* \tag{6.40}$$

we have

$$\lambda = R_c \rho u_*^3 / kg\langle \rho'w' \rangle = R_c L \qquad \text{(highly stable)} \tag{6.41}$$

where L, equal to $u_*^3/(k\langle w'b' \rangle)$, is the Obukhov length, and the proportionality constant R_c has been shown by Zilitinkevich (1975) to be the critical flux Richardson number (the ratio of buoyancy to shear production terms in the turbulent kinetic energy equation). The argument is that the length scale of

turbulence in a highly stratified flow adjusts so that the kinetic energy is roughly in balance with the potential energy gained as eddies overturn.

In summary, there are three length scales that affect vertical turbulent exchange in a steady, horizontally homogeneous RBL: (1) the distance from the ice/ocean (or air/ocean) interface, (2) some fraction of the planetary length scale, u_*/f; and (3) the Obukhov length, which is proportional to the vertical distance a fluid parcel must travel in a stratified fluid in order to convert its kinetic energy to potential energy. The smallest of these length scales will usually determine the turbulence characteristics. A schematic of the turbulence regime is shown in Fig. 6.2. At the surface, there are turbulent stress and buoyancy flux. In the surface layer, the size of the largest and most energetic eddies is controlled by the distance from the surface and, to a lesser extent, by buoyancy effects. The eddies grow until they reach some limiting

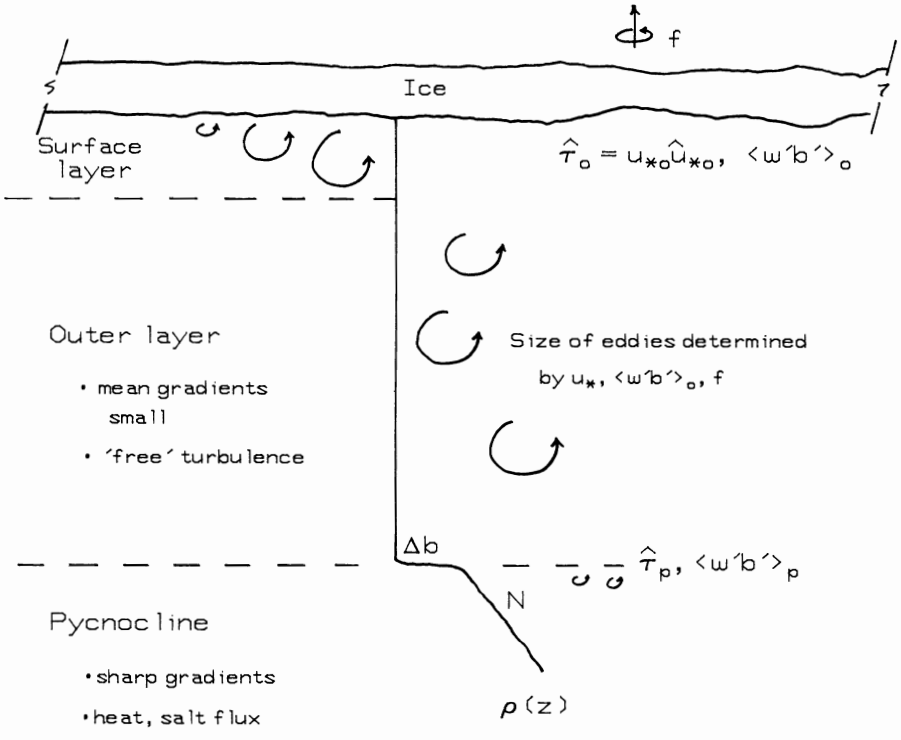

Figure 6.2 Schematic showing the breakdown of the upper-ocean system into three zones: (1) surface layer, eddy size dependent mainly on distance from interface; (2) outer (mixed) layer, eddy size dependent on u_*/f and surface buoyancy flux; and (3) pycnocline, eddy size dependent on stress and buoyancy flux at the interface between the mixed layer and the underlying density gradient.

size in the outer layer determined by the rotation, stress, and surface buoyancy flux. The vertical exchange scale of the largest eddies will be comparable to the surface layer thickness, and they will extend through the boundary layer to some level determined either by Coriolis-induced attenuation of the turbulent stress or by encountering a preexisting density gradient (pycnocline). If there is turbulent stress at the base of the mixed layer (τ_p), then an eddy flux of heat and salt may occur there ($\langle b'w' \rangle_p$), but gravitational forces associated with a sharp jump in buoyancy across the interface (Δb) and the underlying density gradient (characterized by the Brunt–Väisälä frequency N) will dramatically reduce the size of the eddies.

C. A Heuristic Model for Turbulent Flux in the RBL

A useful tool in fluid dynamics is the concept of similarity, in which a whole class of flows is reduced to one set of equations by nondimensionalizing with carefully chosen scales. A familiar example is wind-tunnel testing of scale airplane models, but the idea is also often applied in rotational boundary layer studies. A method called "Rossby number similarity" has been developed for describing geostrophic wind drag in the neutrally stratified atmosphere (e.g., Blackadar and Tennekes, 1968), in which the scales for stress, velocity, and vertical displacement are u_*^2, u_*, and u_*/f, respectively. We used this nondimensionalization to compare mean flow and turbulence data from the 1972 AIDJEX with atmospheric boundary layer models quite successfully (McPhee and Smith, 1976), even though the actual length scales of the two boundary layers differ by a factor of about 30.

The planetary depth scale of Rossby similarity, u_*/f, and the velocity scale u_* apply only with neutral stratification. When there is positive or negative surface buoyancy flux, the depth scale contracts or expands, with opposing changes in the velocity scale. Compare a case with very rapid melting (analogous to strong radiational cooling in the atmosphere) to one with similar surface stress but little or no buoyancy. In the former, stabilizing buoyancy flux at the surface decreases the vertical exchange scale, so that mixing of heat, salt, and momentum is confined to a thinner layer. The mixed layer shoals, and since momentum is trapped near the surface, currents (including ice velocity) increase. In earlier work (McPhee, 1981, 1983), I proposed a generalization of Rossby similarity for turbulent stress and scalar flux, which includes buoyancy effects and is outlined as follows.

Define the nondimensional variables $\zeta = z/H$ and $\hat{T} = \hat{\tau}/u_{*0}\hat{u}_{*0}$, where H is a characteristic length scale for the RBL and, as before, $u_{*0}\hat{u}_{*0}$ is the vector scale for turbulent stress. The nondimensional, steady-state version of Eq. (6.21) is

$$i\hat{U} = \partial\hat{T}/\partial\zeta \tag{6.42}$$

where $\hat{U}$ is nondimensional velocity,

$$\hat{U} = \frac{fH}{u_{*0}} \cdot \frac{\hat{u}}{\hat{u}_{*0}} \tag{6.43}$$

First-order closure in nondimensional variables is

$$\hat{T} = K_* \, \partial \hat{U} / \partial \zeta \tag{6.44}$$

where

$$K_* = K/fH^2 \tag{6.45}$$

so that differentiation of Eq. (6.42) leads to a second-order, ordinary differential equation for turbulent stress:

$$(i/K_*)\hat{T} = d^2\hat{T}/d\zeta^2 \tag{6.46}$$

To find the depth scale H we consider a combination of the maximum exchange scales given by Eqs. (6.36) for the neutral RBL and (6.41) for the highly stable RBL. A simple function which satisfies the two limits is

$$\lambda_m = \xi_N u_{*0} \eta_*^2 / f \tag{6.47}$$

where

$$\eta_* = \left(1 + \frac{\xi_N u_{*0}}{f} \cdot \frac{1}{R_c L}\right)^{-1/2} \tag{6.48}$$

The nondimensional eddy viscosity is

$$K_* = k u_{*0} \lambda_m / fH^2 = k\xi_N \tag{6.49}$$

in which the last equality comes from the stipulation that the nondimensional eddy viscosity is the same for all solutions, including neutral. Thus

$$H = u_{*0}\eta_*/f \tag{6.50}$$

Since we are considering turbulent stress, variation of K within the surface layer is relatively unimportant (see, e.g., Fig. 1 of McPhee, 1981), and as a first-order approximation we assume that eddy viscosity through the entire boundary layer is constant, $K_* = k\xi_N$. The solution of Eq. (6.46) with boundary conditions $\hat{T}(0) = 1$ and $\hat{T}(-\infty) = 0$ is

$$\hat{T} = e^{\hat{\delta}\zeta} \tag{6.51}$$

where

$$\hat{\delta} = (i/K_*)^{1/2} \tag{6.52}$$

This remarkably simple expression for momentum flux in the boundary layer contains many features found both in boundary layer data and in more

sophisticated numerical models (see the comparison in McPhee, 1987). With increasing depth, the complex exponential both rotates *(cum sole)* and diminishes the magnitude of the horizontal stress vector. An important consequence of the extended similarity theory is that, since profiles of momentum flux are similar for all neutral and stably stratified RBLs, it can predict how deep turbulence will penetrate (and thus mix conserved properties) under varying conditions of surface stress and surface buoyancy flux. We refer to this depth as the dynamic RBL depth, to distinguish it from the mixed-layer depth (which may reflect, say, previous conditions of much different surface forcing). For the neutral atmospheric planetary boundary layer (PBL), estimates of the nondimensional dynamic boundary layer depth vary from around 0.25 to 0.6. Using observations of freshening of the upper ocean during the melt season at the AIDJEX camps, I found the nondimensional dynamic depth to be about 0.4 (McPhee, 1986b). Using this value, the dynamic boundary layer depth for high latitudes ($f = 1.4 \times 10^{-4}$ s^{-1}) is plotted for u_{*_0} ranging from 0.5 to 1.5 cm s^{-1} (stress ranging from

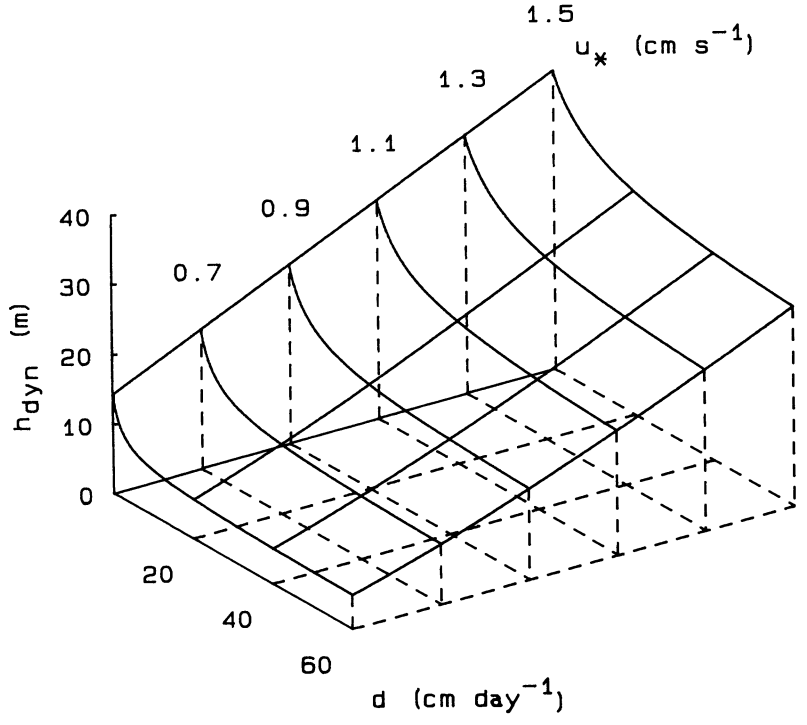

Figure 6.3 Perspective view of dimensional dynamic boundary layer depth, i.e., the maximum depth of active turbulent mixing, for melt rates ranging from 0 to 60 cm day^{-1} and stress ranging from 0.03 to 0.23 Pa.

0.025 to 0.23 Pa) and ice melt rates from 0 to 60 cm day^{-1} in Fig. 6.3. The depth of frictional influence decreases rapidly with melt rate, especially with small to moderate turbulent stress.

The heuristic arguments may be extended to include a pycnocline as follows. Consider the stress profile in an idealized system comprising a well-mixed layer with eddy viscosity K overlying a stable pycnocline, with turbulence characterized by a much smaller eddy viscosity K_p as sketched in Fig. 6.2. To simplify matters, we ignore the buoyancy jump Δb but note that it is straightforward (but algebraically messy) to reinstate it.

We have introduced a new physical length scale: the mixed-layer depth $-z_p$. When the layer is thin relative to the dynamic boundary layer depth ($z_p > z_{dyn}$), turbulence may be intense at the mixed-layer/pycnocline interface, but its exchange scale will be substantially reduced by the density gradient. This will affect both the current structure (and ice drift) of the system and the rate at which denser water is entrained into the mixed layer from below. On the other hand, if the existing mixed-layer depth is greater than the dynamic depth and if there is positive surface buoyancy flux, a new, shallower mixed layer will begin to form at z_{dyn}. During the melt season, the polar mixed layer thus progresses through a series of steps in salinity and temperature structure as the interplay between wind and melt rate dictates how the layer shoals or deepens (see McPhee, 1986b).

With the same RBL scales as before, the nondimensional stress profile is obtained by matching stress and velocity (which is proportional to the derivative of stress) at the nondimensional pycnocline level ζ_p (see McPhee, 1986b, 1988)

$$\hat{T}(\zeta) = \begin{cases} 2\hat{A}\sinh(\hat{\delta}\zeta) + e^{-\hat{\delta}\zeta}, & \zeta \geqslant \zeta_p \\ \hat{T}_p\, e^{\hat{\gamma}(\zeta-\zeta_p)}, & \zeta < \zeta_p \end{cases}$$

$$\hat{A} = \frac{(\hat{\gamma}+\hat{\delta})e^{-\hat{\delta}\zeta_p}}{2[\cosh(\hat{\delta}\zeta_p) - \hat{\gamma}\sinh(\hat{\delta}\zeta_p)]} \tag{6.53}$$

where $\hat{\gamma} = (i/K_{*_p})^{1/2}$, K_{*_p} is the eddy viscosity in the upper part of the pycnocline, and $\hat{T}_p$ is nondimensional stress at ζ_p.

When the system is entraining (i.e., actively mixing at z_p), the key to estimating flux is the length scale of turbulence for K_{*_p}. We assume that stratification is always sufficient to force turbulence to scale with the local Obukhov length

$$K_p = k u_{*_p} R_c L_p \tag{6.54}$$

where

$$L_p = u_{*_p}^3 / k\langle b'w'\rangle_p \tag{6.55}$$

and

$$u_{*_p}\hat{u}_{*_p} = \hat{T}_p u_{*_0}\hat{u}_{*_0} \tag{6.56}$$

Assuming the eddy diffusivity for scalar flux is proportional to eddy viscosity, the buoyancy flux may be written in terms of mean quantities

$$\langle b'w'\rangle_p = -\alpha K_p \left.\frac{\partial b}{\partial z}\right|_p = \alpha N^2 K_p \tag{6.57}$$

where α is the ratio of scalar eddy diffusivity to eddy viscosity (the inverse turbulent Prandtl number) and N the buoyancy frequency in the upper pycnocline. Substituting into Eq. (6.54) and nondimensionalizing, we have

$$K_{*_p} = \frac{fK_p}{(u_{*_0}\eta_*)^2} = \sqrt{\frac{R_c}{\alpha}}\frac{f}{N}\frac{T_p}{\eta_*^2} \tag{6.58}$$

Combining Eqs. (6.58) and (6.53) provides an implicit equation for the one unknown, T_p, which can be solved by iteration.

The ratio α varies from unity (or possibly higher) in fully developed turbulence to quite small values in very stable flows (see Turner, 1973, Figure 5.13). I was able to simulate summer AIDJEX data reasonably well with a constant value of 0.1 (McPhee, 1986b). When the mixed layer is very shallow, α is probably larger (McPhee, 1987).

When the surface buoyancy flux is negative (freezing), the Obukhov length is negative, and η_* is larger than unity. An *ad hoc* extension of the similarity model to unstable conditions allows the turbulent exchange scale to grow with increasing η_*, following Eq. (6.48), until it reaches $|z_p|$. Unlike situations where a large expanse of ice can overrun warm water and melt very rapidly, freezing rates are limited by heat conduction through the ice, which slows rapidly as ice thickness increases. We thus expect surface buoyancy flux due to freezing to have a relatively small impact on RBL dynamics; however, an exception may occur if an expanse of water exposed to cold temperature is continually swept clear of newly formed ice by the wind.

Mean profiles of velocity, temperature, and salinity are obtained by integrating their respective flux profiles. Nondimensional velocity, for example, is found by integrating Eq. (6.53) through the layers shown schematically in Fig. 6.2. Below the dynamic depth, $\hat{U}$ is zero, so in the pycnocline

$$\hat{U}(\zeta) = -i\hat{\gamma}\hat{T}_p e^{\hat{\lambda}(\zeta-\zeta_p)}, \qquad \zeta < \zeta_p \tag{6.59}$$

In the well-mixed outer (Ekman) layer

$$\hat{U}(\zeta) = \hat{U}(\zeta_p) - i\hat{\delta}[2\hat{A}\cosh(\hat{\delta}\zeta) - e^{-\hat{\delta}\zeta}], \qquad \zeta_p \leq \zeta \leq \zeta_{sl} \tag{6.60}$$

where $-\zeta_{sl}$ is the nondimensional depth of the surface layer. For the mean velocity profile, variation of eddy viscosity in the surface layer is important,

since much of the shear takes place in the logarithmic layer near the interface. We define the surface layer depth by the level at which the distance from the surface is equal to the limiting exchange scale λ_m [Eq. (47)]. For smaller distances, the exchange scale is equal to the depth, so the nondimensional surface layer extends to

$$\zeta_{sl} = -\eta_* \xi_N \tag{6.61}$$

in which the eddy viscosity is

$$K_* = -k\zeta/\eta_* \tag{6.62}$$

For $|\zeta|$ small, nondimensional stress can be expressed by a Taylor series expansion

$$\hat{T} = 1 + \hat{\delta}\zeta \tag{6.63}$$

so that

$$\hat{U}(\zeta) = \hat{U}(\zeta_{sl}) - \frac{\eta_*}{k} \int_{\zeta_{sl}}^{\zeta} \left(\frac{1}{\zeta'} + \hat{\delta} \right) d\zeta', \qquad \zeta > \zeta_{sl} \tag{6.64}$$

The integrand is ill behaved as ζ approaches zero, so the upper limit of integration is taken as the nondimensional surface roughness

$$\zeta_0 = -fz_0/(u_{*0}\eta_*) \tag{6.65}$$

and surface velocity is given by

$$\hat{U}_0 = \hat{U}(\zeta_{sl}) + \frac{\eta_*}{k} \left[\ln \left(\frac{\zeta_{sl}}{\zeta_0} \right) + \hat{\delta}\zeta_{sl} \right] \tag{6.66}$$

Equation (6.66) is a generalized drag law for sea ice, which expresses the surface velocity relative to the undisturbed geostrophic flow as a function of the friction velocity at the interface, the buoyancy flux at the interface, the depth of the mixed layer, and the strength of stratification below the mixed layer.

To recapitulate, the equations for stress and velocity as a function of depth in the steady RBL are solved by matching stress and velocity at the base of the mixed layer to derive an implicit equation for T_p, the nondimensional stress magnitude at ζ_p, which is solved by iteration. Velocity is obtained by integrating the stress divided by eddy viscosity through three separate layers representing the pycnocline, the mixed (Ekman) layer, and the logarithmic surface layer. Profiles of temperature and salinity may be obtained in a completely analogous way, except that a laminar/transition sublayer adjacent to the ice/ocean interface must also be considered, as discussed in Section VI.

The calculations are simplified if stratification can be ignored. If the mixed layer is deep and melting or freezing is slow (a situation that pertains to the central Arctic much of the year), then nondimensional stress is given by Eq. (6.51) and surface velocity is

$$\hat{U}_0 = -i\hat{\delta}(1 - \hat{\delta}\xi_N) + \frac{1}{k}\left(\ln \frac{\xi_N u_{*0}}{f z_0} - \hat{\delta}\xi_N\right) \tag{6.67}$$

Grouping terms, we have the Rossby similarity drag law expressed in complex form:

$$\hat{U}_0 = \frac{\hat{u}_0}{\hat{u}_{*0}} = \frac{1}{k}([\ln \mathrm{Ro}_* - A] - iB) \tag{6.68}$$

where $\hat{u}_0$ is the surface (ice) drift velocity relative to the surface geostrophic flow, $\mathrm{Ro}_* = u_{*0}/fz_0$ is the "surface friction Rossby number," and

$$\begin{aligned} A &= \left(1 - \ln \xi_N - \sqrt{\frac{k}{2\xi_N}} + \sqrt{\frac{\xi_N}{2k}}\right) \cong 2.2 \\ B &= \sqrt{\frac{k}{2\xi_N}} + \sqrt{\frac{\xi_N}{2k}} \cong 2.3 \end{aligned} \tag{6.69}$$

Various effects of rotation and buoyancy on the turbulent stress and mean velocity of the boundary layer are demonstrated in Fig. 6.4, for a fixed interfacial kinematic stress of 1 $\mathrm{cm^2\ s^{-2}}$ directed along the y axis, with $z_0 =$ 0.06 m. For case (a) there is no stratification in the water column, the mixed layer is at its freezing temperature, and there is no melting. Both stress and velocity spiral clockwise downward, with velocity leading by 45° in the neutral Ekman layer below the surface layer (which extends down about 3.7 m). At the interface, the surface current (which is ice velocity) is 13.5 cm $\mathrm{s^{-1}}$, directed 23° to the right. Case (b) is like case (a) except that a pycnocline with constant density gradient ($N = 0.02\ \mathrm{s^{-1}}$) is imposed below 15 m. Stress is confined mainly to the mixed layer. Below the surface layer, currents are relatively uniform at right angles to the surface stress, down to the pycnocline, at which there is large shear in both speed and direction. Surface velocity is slightly retarded relative to the neutral RBL and directed a few degrees farther to the right. The level of stress at 15 m suggests that active entrainment is occurring. Case (c) is like case (b) except that the mixed-layer temperature is set to 3°C, which gives rise to a melt rate (see Section VI) of about 27 cm $\mathrm{day^{-1}}$. The ice drifts about 25% faster and 6° farther to the right. Note also that current structure in the mixed layer is much less "slablike," as buoyancy reduces the vertical scale of the RBL, in effect pushing the pycnocline deeper in nondimensional coordinates.

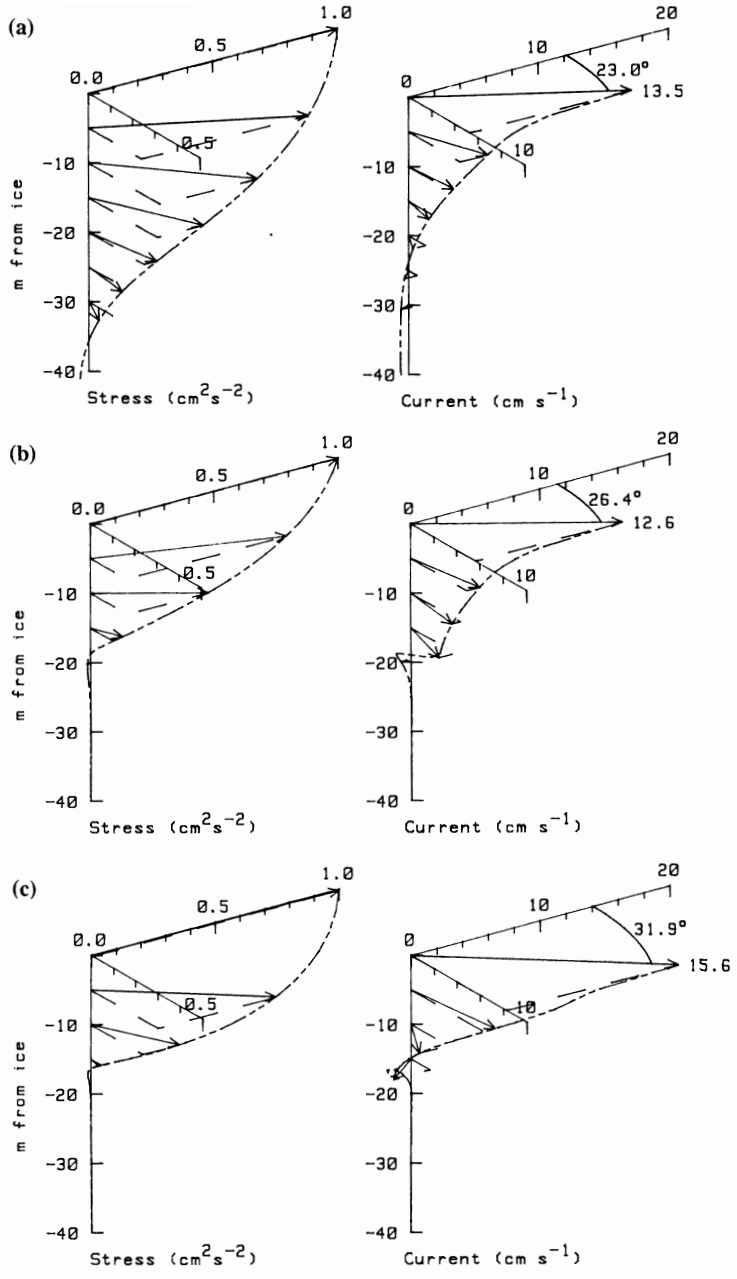

Figure 6.4 Implicit-analytical model hodographs of Reynolds stress and mean current for (a) no surface buoyancy flux (the mixed layer is at its freezing temperature), no pycnocline; (b) no surface buoyancy, pycnocline at 15 m; (c) mixed-layer temperature set to 3°C, pycnocline at 15 m. Numbers at surface indicate surface speed in centimeters per second and boundary layer turning angle.

IV. Some Measurements from the Under-Ice Boundary Layer

A sample of measurements from under-ice RBL studies helps illustrate some of the concepts developed in the previous section. Figure 6.5, from the 1972 AIDJEX Pilot Study (McPhee and Smith, 1976), provides another good example of spiral-like structure in mean currents, this time from a composite average of 5 h of data during a particular storm. Currents are drawn relative to flow measured by an instrument cluster 32 m below the ice/ocean interface, which was near the base of the mixed layer, with the x axis aligned along the direction of shear between the ice and the 2-m level. Note that the integrated volume transport through the boundary layer is almost all in the y direction, i.e., at right angles to the interfacial stress. We found that this integral implied a stress of about 0.29 Pa [see Eq. (6.23)], whereas direct turbulence measurements indicated local turbulent stress at the interface to be about 0.1 Pa, and argued that the difference was due mainly to pressure gradients associated with under-ice topography, i.e., form drag on ridge

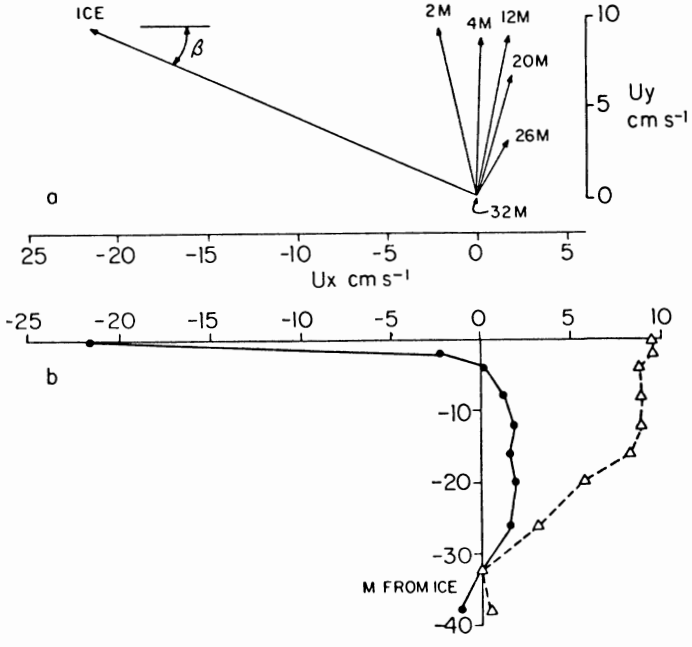

Figure 6.5 Mean current hodograph and profiles relative to 32 m below the ice during a storm at AIDJEX 72 Pilot Study. In a frame of reference drifting with the ice, the relative current at 32 m was within 2 cm s^{-1} of the apparent bottom velocity. Reprinted with permission from McPhee (1986b); copyright by Plenum Press.

keels. Profiles of the diagonal components of the Reynolds stress tensor, scaled by u_* and u_*/f, where u_* was estimated from turbulent stress measurements, are shown in Fig. 6.6. The sum of the three components is twice the turbulent kinetic energy per unit mass. The measurements are shown with results from two numerical models of the neutrally stable atmospheric boundary layer: the second-order closure model of Wyngaard *et al.* (1974) and averaged results from the LES model of Deardorff (1972).

Similar measurements in the marginal ice zone of the Greenland Sea are shown in Fig. 6.7, from McPhee *et al.* (1987). Here, velocity vectors averaged over 3.5 days are drawn relative to drifting ice (measurement reference frame), along with the average results of a time-dependent, numerical model based on the scaling concepts introduced in Section III. During this time, the mixed-layer depth varied between 10 and 20 m. Observed and modeled velocity hodographs differ in some details, but their overall similarity is striking. The relatively shallow pycnocline exerts strong influence on the mean velocity structure, as can be seen by comparison with Fig. 6.5, for which the mixed-layer depth was 30–35 m.

Figure 6.8 shows the measured and modeled Reynolds stress vectors for the same period. Contrary to the turbulence model, measured turbulent

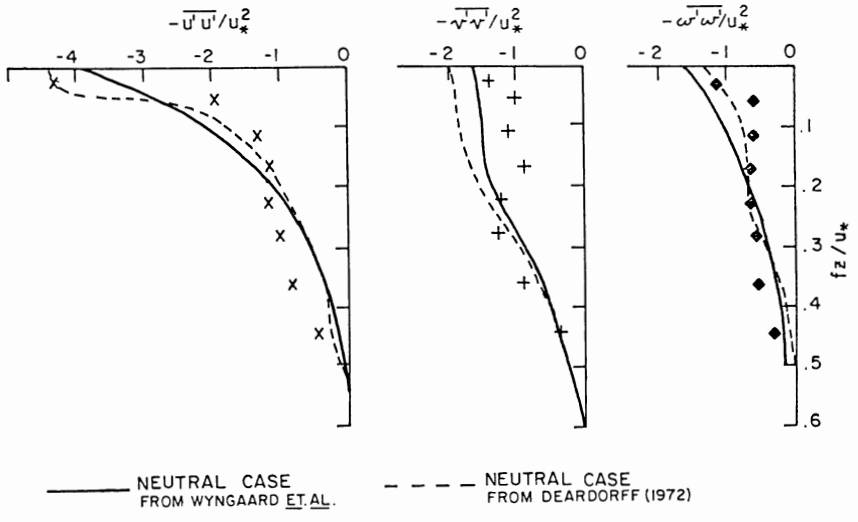

Figure 6.6 Profiles of the diagonal components of Reynolds stress at eight depths ranging from 2 to 32 m in the boundary layer for the same period as Fig. 6.5, nondimensionalized by u_* as determined from near-surface stress measurements. Curves are corresponding predictions from the atmospheric models of Wyngaard *et al.* (1974) and Deardorff (1972). Reprinted with permission from McPhee and Smith (1976); copyright by the American Meteorogical Society.

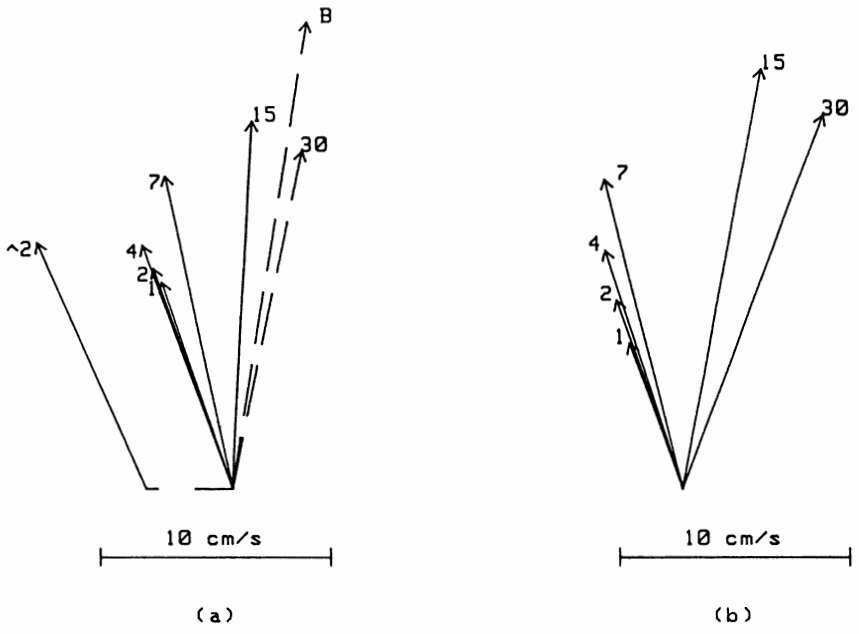

Figure 6.7 (a) Average current hodograph from an 84-h storm during MIZEX 84 in the Greenland Sea. North is up. Numbers indicate depth from the ice underside, with the vector labeled "^2" from a cluster about 100 m away from the main turbulence mast. Vectors labeled "30" and "B" are, respectively, the average 30-m velocity from a profiling system and the apparent bottom velocity from satellite navigation. (b) Averaged results from a time-dependent numerical model forced by observed wind stress, transformed into the drifting reference frame. Reprinted from McPhee *et al.* (1987); copyright by the American Geophysical Union.

stress decreases as the ice/ocean interface is approached. We argued that this resulted from the nonuniform nature of roughness elements on the ice underside, with larger elements contributing to the Reynolds stress observed in the middle and outer regions of the mixed layer but not to the stress measured near the interface under smooth ice. As discussed in the next section, resolving how total drag is partitioned into skin friction, overall turbulent stress, and form drag warrants additional research.

A surprisingly different RBL is shown in Fig. 6.9, from data taken with a frame of equally spaced turbulence clusters under ice near the center of the AIWEX camp in April 1985. The upper cluster on the frame was positioned 2 m below the interface, and data were gathered for about 2 h during a steady drift. The velocity hodograph on the left shows near-surface currents roughly comparable to the MIZEX measurements of Fig. 6.7, but stress magnitudes

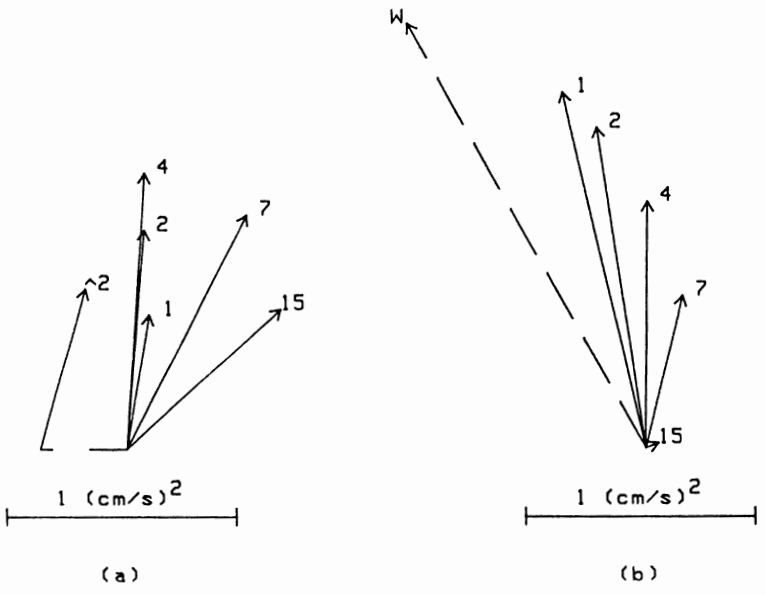

Figure 6.8 As in Fig. 6.7, except (a) measured Reynolds stress and (b) modeled turbulent stress. Reprinted McPhee *et al.* (1987); copyright by the American Geophysical Union.

(right-hand hodograph) are at least five times smaller than at the MIZEX site (Fig. 6.8). The mixed layer was 20–25 m thick and very close to neutrally stable at AIWEX; so I estimated the interfacial friction velocity u_{*0} by fitting (in a least root-mean-square sense) the measured stress at each level, nondimensionalized by interfacial stress, to the simple exponential given by Eq. (6.51). The stress hodograph drawn is the result, with surface stress aligned with the relative current at 2 m. Despite the short averaging time and small magnitudes (of order 0.01-Pa actual stress), the measurements fit the simple exponential quite well.

The stress at the interface is so small that a Reynolds number based on u_{*0} and z_0 [derived from Eq. (6.35)] fell within a range for which the surface is considered hydraulically smooth (see Hinze, 1975, Chapter 7). Under these conditions, the RBL no longer depends on surface roughness, and we may replace the logarithmic part of the surface layer velocity in Eq. (6.66) (with $\eta_* = 1$) by Hinze's empirical result, namely

$$U_s = 2.44 \ln (u_{*0}|z_{sl}|/\nu) + 4.9 \tag{6.70}$$

where ν is kinematic molecular viscosity and

$$z_{sl} = -u_{*0}\xi_N/f \tag{6.71}$$

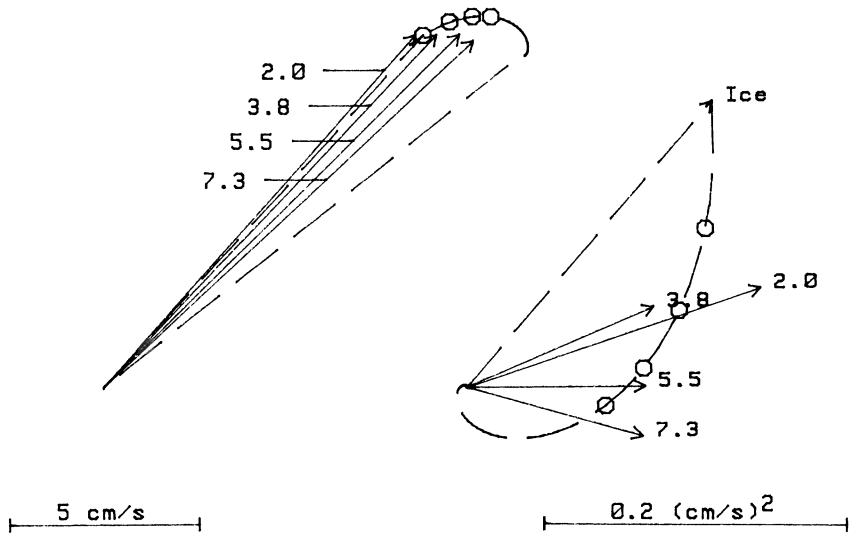

Figure 6.9 Hodographs of mean current and stress measured relative to the ice during AIWEX 85 in the Beaufort Sea. The theoretical curves are from a simple exponential stress model fitted to the observations, with velocity obtained by assuming the surface to be hydraulically smooth.

The model velocity hodograph constructed in Fig. 6.9 thus depends only on u_{*0}, and the measurements are remarkably close to an ideal, hydraulically smooth, rotating boundary layer.

Finally, direct measurements of vertical turbulent heat flux ($\langle w'T' \rangle$) in the RBL are shown in Fig. 6.10, from McPhee *et al.* (1987). During the MIZEX 84 drift, the ice crossed an abrupt mixed-layer temperature front, after which bottom melting increased rapidly. Figure 6.10 shows the average heat flux from all turbulence clusters within the mixed layer, along with a melt rate derived from once-daily measurements of bottom elevation at several sites surrounding the turbulence experiment. The heat flux and melt rate scales are equivalent if we assume that all of the upward heat flux melts ice, where the latent heat of melting is adjusted for brine volume (see Section VI). The dashed curve marked by crosses is from a simple model based on mixed-layer temperature and salinity and u_{*0}, described in Section VI.

V. Drag Coefficients and Under-Ice Roughness

Much of the previous discussion of RBL dynamics may seem esoteric to a reader who simply wants to know: what is the drag of the ocean on drifting

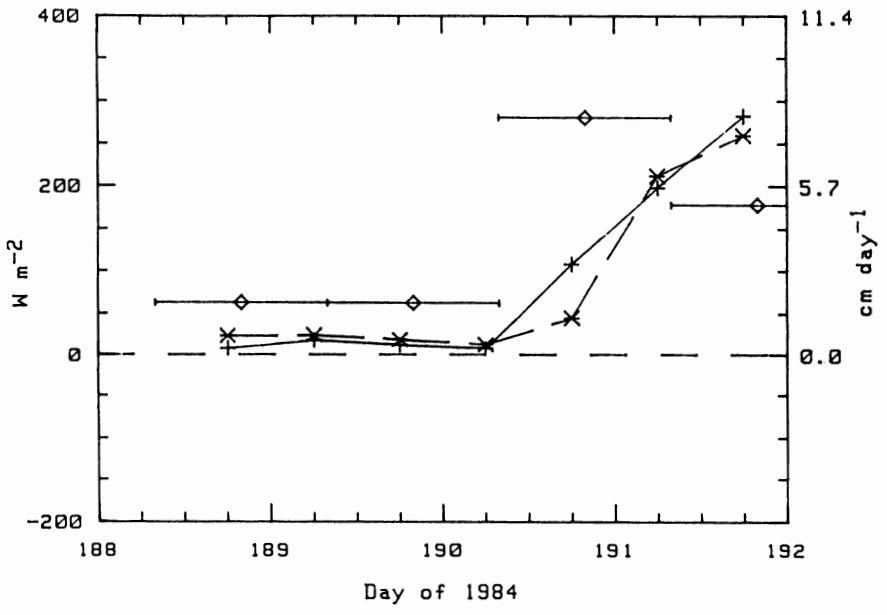

Figure 6.10 Vertical turbulent heat flux in watts per square meter during the MIZEX 84 drift of Fig. 6.7. Solid curve marked "+" is the average of all $\langle w'T' \rangle$ determinations in the mixed layer; dashed curve marked "×" is from the heat flux model described in Section VI; solid bars with diamonds are daily average bottom melt rates in centimeters per day, from ablation stakes surrounding the turbulence mast. Reprinted from McPhee *et al.* (1987); copyright by the American Geophysical Union.

sea ice? But, like the proverbial one-armed economist, an oceanographer who answers quickly risks oversimplifying a complex set of problems. First, there are a number of differing meanings and concepts concerning under-ice drag, so precise definition is difficult; and second, there are factors such as buoyancy and internal wave drag that, for ice with given roughness and velocity, can drastically modify momentum flux to the ocean. There have been several determinations of interfacial stress, drag coefficients, and under-ice surface roughness for drifting sea ice. In this section, the methods and results are discussed and compared in a common context.

Since actual shear stress on the ice undersurface is rarely, if ever, measured directly, its value is inferred from other measurements. We thus require some "model" of how measurable quantities are related to the actual stress, and often uncertainty in our theoretical methods is at least as important as the accuracy or statistical significance of our measurements. Several methods for determining ice/ocean stress have been used, including (1) profiles of mean current in the "logarithmic" layer, (2) direct measurements

of turbulent (Reynolds) stress, (3) measurements of total transport in the RBL (momentum integral method); (4) combining turbulent stress measurements with mean velocity measurements; and (5) inferring stress indirectly as a residual in the balance of forces acting on the ice.

Before describing the methods, it is pertinent to discuss what comprises "interfacial stress." Three potentially major contributors to the total momentum flux between ice and ocean have been identified from observations: "skin friction" arising from turbulence associated with shear in the boundary layer, "form drag" on objects (like pressure ridge keels) that protrude well beyond the general roughness elements characteristic of the under-ice surface, and momentum flux out of the ice/RBL system in the internal wave field. The last, discussed in Section VII, is important only when there is strong stratification near the surface, which is rare except in marginal ice zones. Of the five methods mentioned above, only the last includes a measure of internal-wave stress.

The distinction between skin friction and form drag is meaningful under conditions which seem to typify much of the perennial Arctic ice pack, where reasonably flat and uniform floes are bounded by pressure ridges separated by distances which are large compared with the size of the ridges. Using the analogy implied by the planetary (u_{*0}/f) length scaling, we may view flow in the RBL under pack ice with pressure ridge keels every few hundred meters as a scale model of mid-latitude atmospheric flow over fairly uniform terrain punctuated every few kilometers by low hills. In the latter, the flow will be disturbed in the vicinity of the hills and a net pressure on each hill will add to the downward momentum flux, increasing the total drag on the atmosphere. However, if we measured turbulent stress in the surface layer somewhere on the flat between hills, we would not detect the form drag stress. A similar situation often applies to sea ice, but when the larger roughness features are closely spaced, disturbances from each blend with the others and the distinction between turbulent skin friction and form drag blurs. Measurements near the interface may then show less of the actual turbulent flux than is apparent farther into the boundary layer at the same location. We suggested (McPhee *et al.*, 1987) that this was the reason for the increase in stress observed in the first few meters under the MIZEX floe.

A. Surface Layer Profile Measurements

Surface layer profile techniques follow directly from the law of the wall, Eq. (6.35). If current speed relative to the ice is measured at two levels, z_1 and z_2, in the surface layer, stress is calculated from

$$u_{*0} = k(u_2 - u_1)/\ln(z_2/z_1) \tag{6.72}$$

and surface roughness is

$$z_0 = \exp\left(\frac{u_2 \ln|z_1| - u_1 \ln|z_2|}{u_2 - u_1}\right) \tag{6.73}$$

The drag coefficient applicable to relative current measured at a particular level in the flow, $z = h$, is related to surface roughness by

$$c_h = \left(\frac{1}{k} \ln \frac{|h|}{z_0}\right)^{-2} \tag{6.74}$$

Untersteiner and Badgley (1965), Johannessen (1970), Ling and Untersteiner (1974), and Pease *et al.* (1983) cite either drag coefficients or surface roughness lengths calculated by the "log profile" method. Although easily applied, the technique has several drawbacks. First, the disparity in scales makes the surface layer in the ocean roughly 30 times thinner than the atmospheric surface layer, so the assumption of constant stress out to realistic measurement levels is suspect. It turns out that this is not as restrictive as it might seem, since the relative speed profile remains approximately logarithmic for some distance past the surface layer. On the other hand, since measurements are made at the edge or beyond the surface layer, stability effects need to be considered carefully. Unless properly accounted for, a melt rate as low as a couple of centimeters per day can have a significant impact on stress estimated from the mean profile out to 5 m. Also, since the method is confined to measurements in or near the surface layer, it fails to include any estimate of form drag effects.

B. Direct Measurements of Reynolds Stress

With the proper equipment, we can measure turbulent fluctuations in the flow under the ice and, from a statistical treatment, estimate the momentum flux at a given level directly. Interfacial stress is inferred from the Reynolds stress. Examples of Reynolds stress measurements are given by Smith (1974), McPhee and Smith (1976), Langleben (1980, 1982), McPhee *et al.* (1987), and McPhee (1989).

Langleben used a three-axis ultrasonic current meter to measure mean and turbulent velocities 1 m below the ice at AIDJEX station Caribou, located on a floe in the multiyear pack over the Canadian basin. He later measured stress 1 m below undeformed first-year ice in Barrow Strait, Northwest Territories. In both cases, he found quite small values for the drag coefficients (in fact, the measurements in Barrow Strait imply a hydraulically smooth surface), which again pose the surface layer dilemma: if the measurements are close enough to be considered within the constant-stress

layer, they are probably too close to pick up turbulence generated by larger but sparser roughness elements (see, e.g., the MIZEX stress hodograph in Fig. 6.8).

C. Momentum Integral Methods

A distinctly different approach uses Eq. (6.23) to estimate the total stress including form drag by integrating the volume transport through the boundary layer from a level at which stress is assumed to be zero. For currents averaged over an inertial cycle, the time derivative is often negligible. While the method in principle includes the contribution from keel form drag (Hunkins, 1975), it is valid only if averaged over an area that encompasses features responsible for the form drag. In other words, profiles from a single location may be unduly influenced by local under-ice topography. I cited an example from AIDJEX 72 (McPhee, 1974) in which surface stress calculated from simultaneous current meter profiles, spaced about 110 m apart, varied by a factor of $2\frac{1}{2}$, despite similar surface layer behavior and roughly the same amount of RBL turning. The difference came in the shape of the cross-stress profiles and in the choice of reference level.

D. Combination Methods

If stress and velocity are measured at more than one level in the RBL, the added information may be used to refine the estimate of interfacial stress. McPhee and Smith (1976) showed that stress in the near-surface RBL measured during AIDJEX 72 was affected by a local pressure gradient most likely associated with topographic relief. By combining Reynolds stress measurements and the momentum integral of mean velocity between instrument levels, we were able to estimate the magnitude of the pressure gradient term in the momentum equation and adjust our surface stress estimate accordingly.

A variant on this scheme is to formulate a model of RBL stress [such as Eq. (6.51)] and then determine u_{*_0} by fitting observations so as to minimize rms errors, as demonstrated earlier in analyzing the "smooth" RBL of Fig. 6.9.

E. The Force Balance Method

The last method, which can in principle be applied without any measurements from the oceanic RBL at all, consists of deducing the average under-ice stress as a residual in the ice force balance. Expressed in its complex,

steady-state form, the balance is

$$i\rho_i h_i f(\hat{u}_i - \hat{u}_g) = \hat{\tau}_a - \hat{\tau}_0 + \hat{F}_i \tag{6.75}$$

where ρ_i, h_i, and $\hat{u}_i$ are, respectively, ice density, thickness, and velocity; $\hat{\tau}_a$ is tangential air stress; and $\hat{F}_i$ is the sum of forces internal to the ice, usually expressed as the gradient of internal ice stress. The term involving the geostrophic velocity $\hat{u}_g$ comes from the slope of the sea surface, via Eq. (6.18). The internal force term is very difficult to monitor directly, so the best way of applying the technique is to identify situations in which the internal stress must be small, e.g., when ice is thin or divergent, or when inertial oscillation is prominent. Sea surface tilt is also often difficult to measure directly, especially in coastal areas or near frontal regions, so in those cases an accurate measure of relative current just below the RBL is necessary.

Using the force balance method to amass statistics on interfacial stress and relative ice drift for the four AIDJEX stations during the melt season of 1975 (when internal ice forces were small), I found (McPhee, 1979) that the stress/velocity relation was like that predicted by Rossby similarity theory. Of the various drag laws proposed in the literature, only those that incorporated u_*/f scaling agreed with the AIDJEX free drift results (McPhee, 1982). Using a 10-m wind drag coefficient of 0.0027, based on integration of pilot balloon profiles at the AIDJEX sites, and estimating the average ice thickness to be 2.7 m, I found that the surface roughness appropriate for Rossby similarity [see Eq. (6.68)] was about 10 cm, which contrasts sharply with the value of about 0.2 cm inferred from the drag coefficient reported for AIDJEX station Caribou by Langleben (1980), based on direct stress measurements 1 m below the ice.

Pease *et al.* (1983) used an interesting variation on the force balance theme to estimate both air and water drag coefficients directly from measured surface wind, measured current in the under-ice surface layer, ice velocity, and estimates of geostrophic current. They obtained results similar to those from a current profile analysis done at the same site. Expressed in complex notation, the method is as follows. Let $\hat{u}_0 = \hat{u}_i - \hat{u}_g$ again be the ice velocity relative to geostrophic flow, and use quadratic formulas for air and water stress. If $\hat{F}_i$ is negligible, Eq. (6.75) becomes

$$i\rho_i h_i f\hat{u}_0 = \rho_a c_a u_a \hat{u}_a - \rho c_w u_w \hat{u}_w \tag{6.76}$$

where $\hat{u}_a$ and $\hat{u}_w$ are wind and current relative to the drifting ice. Given accurate measurement of all the velocities and ice thickness, the real and imaginary components of Eq. (6.76) determine the two unknowns c_a and c_w. As Pease *et al.* (1983) point out, if the term on the left side of Eq. (6.76) is small, the force balance is mainly between the two terms on the right, which

are nearly collinear. In this situation, small errors in h_i or $\hat{u}_0$ unduly influence the calculated magnitudes of c_a and c_w, but even so, the method provides a robust estimate of the ratio of the two drag coefficients.

Intuitively, estimates of drag coefficients improve as the Coriolis turning increases, and it is natural to consider the method in the context of the entire boundary layer. It is often convenient to express free drift as a complex ratio of ice velocity (relative to geostrophic flow) to surface wind:

$$\hat{u}_0/\hat{u}_a = re^{-i\theta} \tag{6.77}$$

where θ is the rightward deflection angle with respect to surface wind direction. For the AIDJEX free-drift period (summer 1975), the average ratio for all camps was 0.020 (2%!) with about 47° deflection (McPhee, 1980). During this time the average drift speed (corrected for small geostrophic currents) was about 0.13 m s^{-1}, and from current measurements near the ice we found that the average turning angle in the RBL was about 24°. With this information, it is possible to estimate the surface wind drag coefficient and the geostrophic water drag coefficient, c_g, as a function of ice thickness. We express the wind and water stress in terms of $\hat{u}_0$, so that the steady force balance is

$$i\rho_i h_i f\hat{u}_0 = (\rho_a c_a/r^2)\, u_0\hat{u}_0 e^{i\theta} - \rho c_g u_o \hat{u}_0 e^{i\beta} \tag{6.78}$$

where β is the RBL turning angle. We again decompose the complex equation into components, with the real part expressing the ratio of water and air drag coefficients:

$$c_g/c_a = (\rho_a/\rho r^2)\cos\theta/\cos\beta \tag{6.79}$$

and the imaginary part furnishing the magnitude,

$$c_a = (r^2\rho_i f h_i/\rho_a u_0)(\sin\theta - \cos\theta\tan\beta)^{-1} \tag{6.80}$$

Equation (6.80) implies that for given ice speed, wind drift ratio, and RBL turning (all of which can be readily measured with remote buoys), the drag coefficients are proportional to ice thickness. Unfortunately, mean ice thickness is often quite difficult to estimate, especially over an area large enough to represent the regional force balance. If mean ice thickness in the AIDJEX region is assumed to have been between 3 and 4 m, the corresponding 10-m wind drag coefficient ranges between 0.0021 and 0.0029, with the geostrophic water drag ranging from 0.0049 to 0.0068. These values coincide with the range of independent estimates of air and water drag made for the AIDJEX region. If one or the other of the drag coefficients is known with some confidence, the computation may be inverted to estimate mean ice thickness.

F. A Comparison of Roughness Lengths

Table 6.1 lists a number of independent determinations of under-ice drag, here expressed in terms of the surface roughness length z_0. A number of the cited works report drag coefficients, either referenced to relative current velocity at a particular level or as a "geostrophic" drag. These have been converted to equivalent z_0 values using Eq. (6.74) where a particular level is given [2 m was taken as the reference level for Smith's (1974) drag coeffi-

Table 6.1 Representative Estimates of Undersurface Roughness Length[a]

Source	Location	Method	Reported	z_0 (cm)
Ling and Untersteiner (1974) (after Untersteiner and Badgley, 1965)	Beaufort Sea (Arlis 2)	1	z_0	0.82–1.9
Johannessen (1970)	Gulf of St. Lawrence	1	z_0	3.2
		1	z_0	9.4
	Gulf of St. Lawrence	1	z_0	3.0
	North Pole	1	z_0	0.2
Smith (1974)	Beaufort Sea (Camp 200)	2	c_s	0.13–0.70
McPhee (1974)	Canada Basin (AIDJEX 72)	3	c_g	1.9
Hunkins (1975)	Canada Basin (AIDJEX 72)	3	Stress, u_0	1.1
McPhee and Smith (1976)	Canada Basin (AIDJEX 72)	4	Ro_*	0.08
McPhee (1979)	Canada Basin (AIDJEX 75)	5	z_0	10
Langleben (1980)	Canada Basin (AIDJEX 75)	2	c_1	0.2
Langleben (1982)	Barrow Strait NWT (fast ice)	2	c_1	0.0017
Pease *et al.* (1983)	Bering Sea	1	z_0	8.0
	Bering Sea	5	$c_{1.1}$	5.7–7.4
McPhee (1989)	Greenland Sea (MIZEX)	4	z_0	5.5–7.7
	Beaufort (AIWEX)	4	z_0	Smooth
	Beaufort (PRUDEX)	4	z_0	0.45–0.63
Martinson and Wamser (1990)	Weddell Sea (WWSP-86)	5	c_g	0.06

[a] Method refers to technique used for determining stress: (1) log profile, (2) direct Reynolds stress, (3) momentum integral, (4) combination of direct stress and mean current measurements, or (5) force balance residual. Conversion of drag coefficients to roughness length is described in the text.

cients], or using the rear component of Eq. (6.68) for studies including the entire RBL.

It is difficult to generalize from the results of Table 6.1. The surface layer and direct turbulence measurements do not include the effect of form drag on large pressure ridge keels, yet Johannessen's (1970) second case and my MIZEX example produce very large roughness lengths. The comparison between AIDJEX 72 momentum integral determinations [Hunkins (1975), 1.1 cm; McPhee (1974), 1.9 cm] and the AIDJEX 1975 force balance (10 cm) is interesting because they come from roughly the same geographic region during different years. My force balance estimate is based on a fairly large wind drag coefficient (0.0027) but is consistent with the range of drag coefficients found in the previous subsection for mean ice thickness ranging from 3 to 4 m. In principle, both the momentum integral and force balance methods should account for most of the form drag effect, so the observed increase is probably indicative of a significant increase in ice roughness. It is also interesting that the "marginal ice zone" cases (the second Gulf of St. Lawrence example and the Bering and Greenland Sea examples) are uniformly large. This may be due to processes that tend to break up floes in some more or less similar fashion.

The range of roughness lengths found in Table 6.1 emphasizes the need for more research, both theoretical and observational, on the partition of total drag between skin friction and form drag and on what routine observations can be made to estimate regional values of under-ice roughness.

VI. Heat and Mass Flux at the Ice/Ocean Interface

In the previous sections, momentum flux between the ice and underlying RBL was described in detail. The question asked was essentially: given stress at the interface, what is the velocity of the ice relative to undisturbed water below the boundary layer and how is momentum distributed in the RBL? The inverse question — given relative velocity, what is stress at the ice/ocean interface and how is it distributed? — is just as relevant and is answered in much the same way.

To understand the system fully, we must ask similar questions about fluxes of temperature and salinity and other scalar properties. If we specify the heat and salt flux at the interface (essentially, the ice growth rate), then we should be able to use our knowledge of the dynamics of the RBL to predict changes in its mean temperature and salinity structure. In many practical problems, however, the question is posed in its inverse form: given surface momentum flux and temperature and salinity of the RBL, what is the heat flux (melt rate) at the interface? Stated another way: if an expanse of sea ice is

drifting over a mixed layer that is above freezing, how long will the ice last and how fast will it cool the mixed layer? It appears from recent measurements that the answer is highly dependent on what occurs in a thin layer near the interface and thus has no direct analog in the momentum flux/mean velocity question.

An idealized view of the heat and salt balances at the ice/ocean interface is given in Fig. 6.11, adapted from Mellor *et al.* (1986). We draw an infinitesimal control volume which follows the migrating interface, either up or down according to whether the ice is melting or freezing. From isostasy

$$w = -(\rho_i/\rho)\,\dot{d} = w_0 + w_i \tag{6.81}$$

where $\dot{d}$ is the ice growth rate and ρ_i is ice density. The interface vertical velocity is the sum of w_0, which is due to bottom melting, and w_i, the "percolation" velocity due to water that migrates to the interface from melting in the interior or at the surface of the ice column. The latter is often the

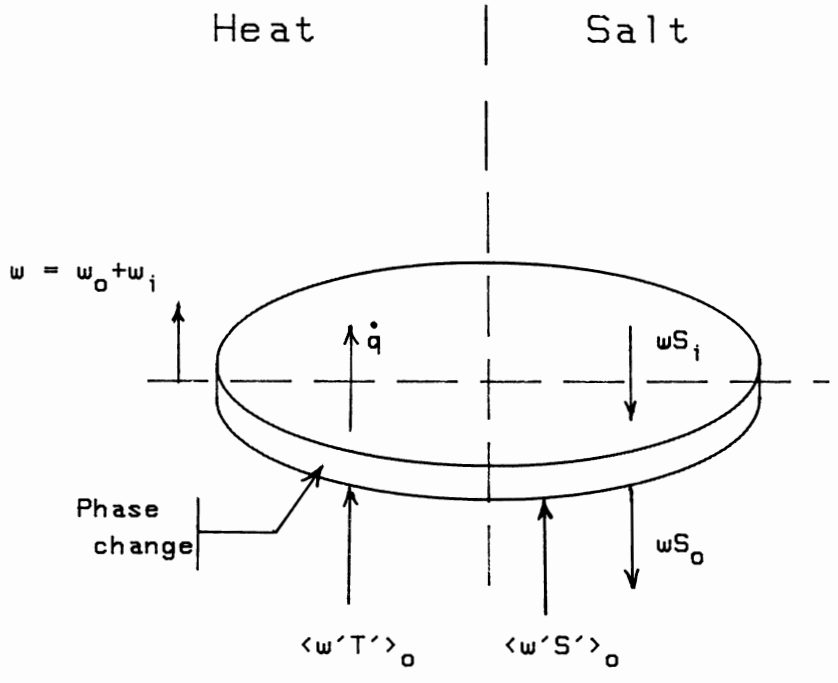

Figure 6.11 Schematic of an infinitesimal control volume following the ice undersurface with vertical velocity w. The heat balance is dominated by conduction through the ice $\dot{q}$; heat flux from the ocean, $\langle w'T'\rangle_0$; and the phase change associated with the bottom melt velocity, w_0. w_i is a "percolation" velocity from melt at the surface and within the ice. The salt budget is a balance between advection and turbulent flux.

major source of buoyancy when ice is compact, and the mixed-layer temperature remains near freezing. We treat it here as uniformly distributed, although it probably occurs in separated drainage channels and at floe boundaries. High melt rates occur when ice overruns warm water (Josberger, 1987); then w may come almost entirely from bottom melting.

The salt balance is shown on the right of Fig. 6.11. If w is positive (melting), fluid with salinity S_i advects into the control volume from above, much saltier fluid with salinity S_0 advects out, and the imbalance is compensated by the upward turbulent flux from the fully turbulent part of the boundary layer

$$\langle w'S' \rangle_0 = w(S_0 - S_i) \tag{6.82}$$

The heat balance is dominated by (a) conduction of heat through the ice, (b) the phase change if bottom freezing or melting occurs, and (c) turbulent heat flux from the ocean. Since sea ice is a mixture of pure ice and brine, its effective latent heat of fusion varies with brine volume, which is a function of temperature and salinity of the ice (Maykut, 1985). For ice that is near the freezing point of typical seawater, this relation is approximately

$$L_S \cong L_0(1 - 0.03S_i) \tag{6.83}$$

where L_0 is the latent heat of pure ice. Neglecting small changes in enthalpy associated with temperature changes in the control volume, the first-law heat balance is

$$\langle w'T' \rangle_0 = w_0 Q_L + \dot{q} \tag{6.84}$$

where

$$\dot{q} = -\frac{k_c}{\rho c_p} \left. \frac{\partial T}{\partial z} \right|_{ice} \tag{6.85}$$

is the heat conduction through the ice (k_c is the thermal conductivity and c_p the specific heat of seawater) and Q_L is the latent heat of fusion (adjusted for brine volume) divided by specific heat, with units of temperature. Water at the immediate interface is at its freezing temperature, related to salinity at the interface by the linear approximation to Eq. (6.32): $T_0 = -mS_0$.

If we assume that the percolation velocity is known (or can be calculated with a model of ice thermodynamics), the fundamental problem of heat and mass transfer at the ice/ocean interface is to relate the bottom ablation rate to mean properties at some level in the fluid. This is a formidable theoretical problem and has been addressed (with widely varying results) by, among others, Josberger (1983), Ikeda (1986), and Mellor *et al.* (1986). McPhee *et al.* (1987) developed a framework for comparing the various approaches, which is briefly recapped here.

Expressing flux as an exchange coefficient times the mean gradient, with Eqs. (6.84) and (6.85), and then integrating from some level z to the surface, the nondimensional changes in temperature and salinity from z to the surface are given by

$$\frac{u_{*0}[T(z) - T_0]}{(w_0 Q_L + \dot{q})} = \Phi_T = \int_z^0 \frac{u_{*0}\, dz'}{\mathscr{K}_h} \tag{6.86}$$

and

$$\frac{u_{*0}[S(z) - S_0]}{(w_0 + w_i)(S_0 - S_i)} = \Phi_S = \int_z^0 \frac{u_{*0}\, dz'}{\mathscr{K}_S} \tag{6.87}$$

where $\mathscr{K}_h$ and $\mathscr{K}_S$ are heat and salt diffusivities, including both turbulent and molecular effects, and u_{*0} is the magnitude of the friction velocity at the interface. Using the freezing-line approximation, Eqs. (6.53) and (6.54) may be combined to obtain a quadratic equation for S_0

$$mS_0^2 + [T_q + (1 + c_1)c_2 - mS_i]S_0 - (T_q + c_2 S_q) = 0 \tag{6.88}$$

where

$$\begin{aligned} c_1 &= \Phi_S w_i / u_{*0}, \qquad c_2 = \Phi_T Q_L / \Phi_S \\ T_q &= T(z) - (\Phi_T / u_{*0})\, \dot{q} \\ S_q &= S(z) + c_1 S_i \end{aligned} \tag{6.89}$$

and thus for the bottom ablation velocity

$$w_0 = \frac{S(z) - S_0}{\Phi_S (S_0 - S_i)}\, u_{*0} - w_i \tag{6.90}$$

McPhee *et al.* (1987) reviewed several approaches to specifying the nondimensional functions Φ_T and Φ_S and found, using heat flux, turbulent stress, and mean T and S measured at 2 m depth during MIZEX 84, that molecular effects dominate the change in T and S across the boundary layer. We suggested that the nondimensional functions can be expressed as a sum of a contribution across the transition/laminar sublayer plus a much smaller contribution across the fully turbulent part of the boundary layer. Standard engineering practice (e.g., Incropera and DeWitt, 1985) and laboratory studies of Yaglom and Kader (1974) indicate an appropriate form of the nondimensional functions for the sublayer region to be

$$\Phi_{T,S} = b \left(\frac{u_{*0} z_0}{\nu}\right)^{1/2} \left(\frac{\nu}{\alpha_{T,S}}\right)^{2/3} + \Phi_{\text{turb}} \tag{6.91}$$

where ν, α_T, and α_S are, respectively, molecular kinematic viscosity, heat

diffusivity, and salt diffusivity. Representative values (Mellor *et al.*, 1986) in square meters per second are $\nu = 1.8 \times 10^{-6}$, $\alpha_T = 1.3 \times 10^{-7}$, and $\alpha_S = 7.4 \times 10^{-10}$. For the MIZEX data, McPhee *et al.* (1987) found the constant in Eq. (6.91) to be $b = 1.6$, about half the laboratory value.

Estimating the turbulent contribution to the nondimensional flux profiles, Φ_{turb} in Eq. (6.91), requires a model for turbulent exchange. A problem often encountered in sea ice studies, especially near the ice margins, is to estimate the bottom melt rate of ice drifting in water above the freezing temperature as a function of interfacial stress, mixed-layer temperature, and mixed-layer salinity. This can be accomplished with a straightforward extension of the similarity concepts discussed in Section III,C. We ignore the pycnocline and assume the Reynolds analogy in the mixed layer. Following closely the derivation of the nondimensional velocity profile in Section III,C (see also McPhee *et al.*, 1987), we have

$$\begin{aligned}\Phi_{\text{turb}} &= \frac{T_{\text{ml}} - T(z_0)}{\langle w'T' \rangle_0 / u_{*0}} = \frac{S_{\text{ml}} - S(z_0)}{\langle w'S' \rangle_0 / u_{*0}} \\ &= \frac{1}{k\xi_{\text{N}}} \int_{-\infty}^{\zeta_{\text{sl}}} e^{a\zeta}\, d\zeta + \frac{\eta_*}{k} \int_{\zeta_{\text{sl}}}^{\zeta_0} \frac{e^{a\zeta}}{\zeta}\, d\zeta\end{aligned} \tag{6.92}$$

where

$$a = \text{Re}(\delta) = 1/\sqrt{2k\xi_{\text{N}}} \tag{6.93}$$

If the integrals are approximated by using a Taylor series expansion for the exponential, and with $|\zeta_{\text{sl}}| \gg \zeta_0$, the result is

$$\Phi_{\text{turb}} = \left(\sqrt{\frac{2}{k\xi_{\text{N}}}} - \eta_* \sqrt{\frac{\xi_{\text{N}}}{2k}} \right) + \frac{\eta_*}{k} \left(\ln \frac{u_{*0}\xi_{\text{N}}\eta_*^2}{fz_0} - \eta_* \sqrt{\frac{\xi_{\text{N}}}{k}} \right) \tag{6.94}$$

where the first term in parentheses is the contribution of the outer layer and the second is from the fully turbulent part of the surface layer. For typical values under sea ice ($u_{*0} = 0.01$ m s^{-1}, $z_0 = 0.05$ m) and with $\eta_* = 1$, Φ_{turb} evaluates to

$$\Phi_{\text{turb}} = 9.6 + 10.1 = 19.7 \tag{6.95}$$

with surface and outer layers contributing about equally. By contrast, the nondimensional changes across the laminar/transition sublayer, given by the first term on the right of Eq. (6.91) with $b = 1.6$, are 153 and 4823 for temperature and salinity, respectively. In other words, the fully turbulent part of the boundary layer contributes less than 12% of the total temperature change and less than 0.5% of the salinity change. Thus a "mixed" layer can exist, even with high surface fluxes, because most of the change in scalar properties occurs across a very thin layer adjacent to the surface.

Steps in using the heat and mass flux model are as follows: (1) specify ice characteristics (w_i, $\dot{q}$, S_i) and forcing environment (u_{*0}, T_{ml}, S_{ml}), (2) evaluate Φ_T and Φ_S using Eq. (6.91) with an initial estimate for η_*, (3) solve the quadratic Eq. (6.88) for S_0 and use this to obtain w_0, and (4) calculate the buoyancy flux from total melt velocity for a refined estimate of η_* and iterate if the change in η_* is significant. This procedure was used to calculate the melt rate of 27 cm day^{-1} in Fig. 6.4c for $u_{*0} = 1$ cm s^{-1}, $T_{ml} = 3°C$, and $S_{ml} =$ 32 ppt ($S_i = 4$ ppt, $w_i = \dot{q} = 0$), demonstrating the effect of high surface buoyancy flux on the stress and velocity profiles.

The MIZEX heat and mass balance studies showed that even with highly turbulent flow near the hydraulically rough ice undersurface, the rate of heat and mass transfer is controlled by molecular processes in a thin layer near the immediate interface. In practical terms, this means that ice can last much longer in water several degrees above freezing than was anticipated using models which neglected the sublayer (Josberger, 1983; Ikeda, 1986). At the immediate ice edge, there is some evidence (Josberger, 1987) that transfer rates are somewhat higher than implied by the "universal" functions of Eq. (6.91); a possible source of higher heat flux there may be enhanced stirring by surface gravity waves.

Figure 6.10 shows results predicted using the model developed in McPhee *et al.* (1987) for drift in above-freezing water compared with actual measurements of heat flux and bottom melt (see also Fig. 18 of Morison *et al.*, 1987).

VII. Internal Wave Drag

Because of the restoring force exerted by gravity, vertical displacement in a stratified fluid is often accompanied by internal waves, which, unlike turbulent processes, are capable of transporting momentum and energy away from the ice/upper-ocean system. In contrast to the open ocean, the ice-covered RBL often has a ready source for internal waves in the form of pressure ridge keels drifting at speeds comparable to internal-wave phase speeds. It has long been speculated that drag from internal waves could be a significant factor in the ice force balance. However, the Arctic Ocean is also noted for the low intensity of its deep internal-wave field (Morison, 1986; Levine *et al.*, 1985); thus we can surmise that, overall, the ice cover probably diminishes rather than enhances internal wave generation.

By extrapolating Ekman's (1906) laboratory studies of "dead-water" drag on a model ship hull to pressure ridge keels, Hunkins (1974) found that for normal ice velocities and 35–50-m-thick mixed layers, internal-wave drag implied by the laboratory model results would be small. Rigby (1974) also

examined internal-wave generation by pressure ridge keels and concluded that the effect was small for typical central Arctic conditions. On the other hand, a set of modern tow tank experiments (Hachmeister and Rigby, 1980; Muench and Hachmeister, 1984) showed that for key parameters typical of the marginal ice zone, internal-wave drag on their model pressure ridges was as great as form drag.

During the last week of the 1984 summer MIZEX project in the Greenland Sea, the behavior of the ice/upper ocean system suggested that internal waves played an important role in RBL dynamics. Figure 6.12a, from Morison *et al.* (1987), shows wind forcing, relative ice speed, and drag coefficient

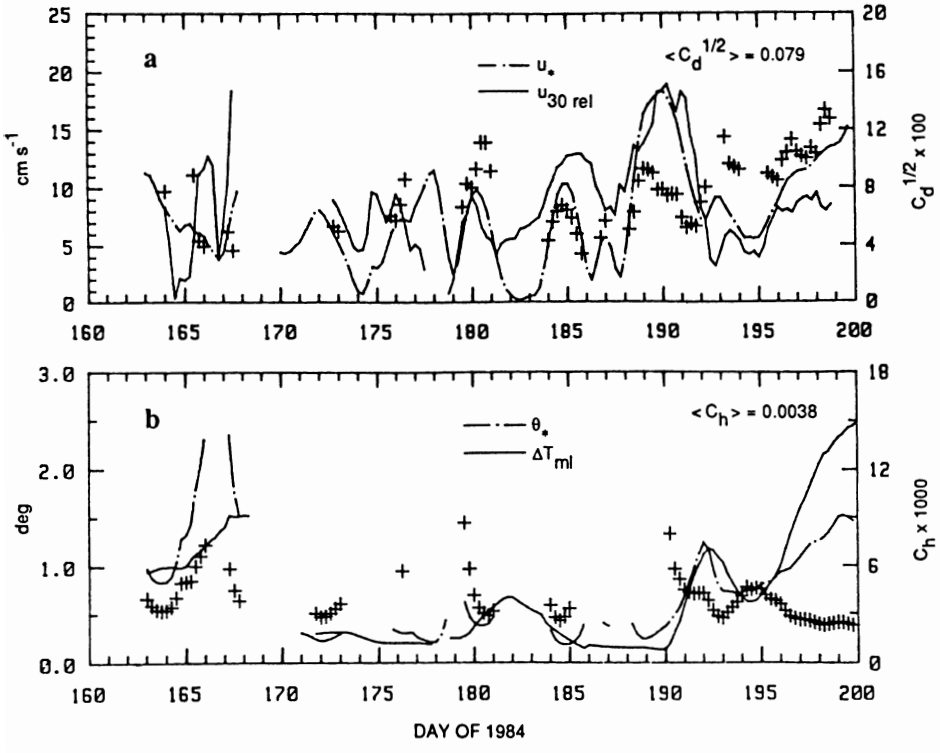

Figure 6.12 (a) Friction velocity determined from wind stress; ice speed relative to 30-m depth; and their ratio, the square root of drag coefficient (+), plotted against time for the entire MIZEX 84 drift in the Greenland Sea. (b) Forcing temperature θ_* (heat flux divided by u_*); elevation of mixed-layer temperature above freezing, ΔT_{ml}; and their ratio, the heat exchange coefficient (+). Reprinted from Morison *et al.* (1987); copyright by the American Geophysical Union.

for the entire drift, where u_* is derived from the wind stress modified by Coriolis acceleration of the ice. Figure 6.12b shows thermal forcing, mixed-layer temperature, and heat transfer coefficient for the entire MIZEX 84 drift. The heat transfer scale θ_* is kinematic heat flux (proportional to bottom melt rate) divided by u_*, and c_h is θ_* divided by mixed-layer temperature. During the last few days, ice was melting in water well above freezing, with stable stratification almost to the interface—conditions for which we would expect strong buoyancy effects. Nevertheless, the drag coefficient was larger than at any other time, while the heat transfer coefficient was smaller. If turbulence had been the only transfer mechanism, buoyancy should have acted to decrease both coefficients, with the largest effect on momentum. Morison *et al.* (1987) argued that momentum flux into the internal-wave field could account for the otherwise peculiar behavior and showed that internal waves with the proper characteristics for significant downward radiation of momentum and energy were present in data from instrument clusters in the upper part of the RBL.

For most practical problems, the length and time scales of internal waves that provide much vertical momentum flux are too small to resolve individually. A parametrization of internal-wave drag on sea ice has been suggested by McPhee and Kantha (1989), based on a two-layer, inviscid theory similar to that described by Gill (1982). Without repeating the complete derivation, our results for one Fourier component of under-ice waviness, characterized by wave number k (which should not be confused with von Karman's constant) and amplitude h_0, expressed the additional drag from internal-wave generation as the product of two factors. The first is the drag that would be encountered if the pycnocline density gradient, characterized by buoyancy frequency N, extended to the ice/ocean interface:

$$c_{wd} = \tfrac{1}{2}k_x^2 h_0^2 \left[(k_c^2/k_x^2) - 1\right]^{1/2} \tag{6.96}$$

where $k_c = N/u_r$ is a critical wave number above which the solutions are evanescent and k_x is the wave number component in the direction of ice motion. This is multiplied by an attenuation factor which takes into account the mixed-layer depth H and the strength of the buoyancy jump at the base of the mixed layer, Δb:

$$\Gamma = \left(\sinh^2(kH)\left\{\left[\coth(kH) - \frac{k\,\Delta b}{u_r^2 k_x^2}\right]^2 + \frac{N^2}{u_r^2 k_x^2} - 1\right\}\right)^{-1} \tag{6.97}$$

The kinematic internal-wave stress is

$$\hat{\tau}_{IW} = -\Gamma c_{wd}\, u_0 \hat{u}_0 \tag{6.98}$$

and acts in addition to the normal RBL turbulent and form drag stress.

The attenuation factor decreases rapidly with increasing mixed-layer depth, so that for H much greater than about 10 m the drag is small. In the central Arctic, the mixed layer is rarely as shallow as 10 m, so internal-wave drag is not often a factor in ice drift. But in the marginal ice zone, rapid melting sometimes leads to extreme stratification and substantial increased drag. This not only slows the ice but also reduces the RBL capacity for turbulent mixing, which both reduces heat flux (bottom melting) and slows mixed-layer deepening.

In McPhee and Kantha (1989), we applied the parametrization in an ice/RBL numerical model, with drag calculated by integrating a plausible spectrum of under-ice roughness over two-dimensional wave number space. We found that a spectrum with a peak wave number of 0.06 m^{-1} (100 m wavelength) and root-mean-square amplitude of 2.0 m produced about the observed amount of increased drag and decreased heat flux. The model also predicted significantly less mixed-layer deepening than a similar model without internal-wave drag, again in agreement with observations. We obtained similar results when we replaced the under-ice waviness spectrum with a single wave number disturbance with the same wavelength and amplitude reduced to 1.4 m. The latter reduces computation significantly.

VIII. Summary

In order to understand (and model) ice motion and thermodynamics, mixed-layer evolution, how physics affects biological processes, and air–ice–sea interaction in general, it is necessary to describe properly what controls fluxes of momentum, heat, salt, and other quantities near the ice/ocean boundary. My experience has been that the problem is usually approached in one of two ways: (1) express the fluxes in terms of bulk exchange coefficients and search for ways of simplifying the physics to specification of a few empirical "constants," or (2) use a computer to solve a numerical model of the conservation equations at multiple levels, in essence relegating the empiricism to smaller and smaller scales, where our knowledge is greatly enhanced by laboratory studies. In some sense, this chapter documents an attempt to strike a middle course, in which we ask: what is the simplest conceptual view of the exchange process that can still account for the important features of the observational base and the results of sophisticated numerical models?

Perhaps the most common question associated with small-scale processes is how much drag the ocean exerts on drifting ice. Studies during the past couple of decades have shown that this is by no means a simple question, nor is it one that we can consider answered. A number of important factors affect

the drag, among which are under-ice roughness, both small and large scale; buoyancy flux at the ice/ocean interface and at the base of the mixed layer; and pressure–displacement correlations in internal waves generated by ridge keels. Similar considerations apply to heat and salt flux between ice and ocean, except that even with very rough ice it appears that much of the gradient in these scalars occurs in a thin layer near the interface where molecular effects are important, often dominant.

Not all of these factors operate all the time. If the mixed layer is deep, internal waves are unlikely to play much role in the ice force balance, and the effect of buoyancy flux at the base of the mixed layer will be minimal. If the mixed layer is near its freezing temperature and the ice is more than a few centimeters thick, it is unlikely that surface buoyancy flux will be of overriding importance in RBL dynamics. Thus, for much of the ice pack in winter, we can probably do an adequate job of describing momentum flux with an expression like Eq. (6.51) and ice velocity relative to the ocean with a Rossby similarity drag law [Eq. (6.68)] (although the question of what value to use for z_0 remains). But the interesting dynamics, thermodynamics, and biology are often associated with areas where many of the factors come into play simultaneously: rapid melting or freezing, changes in upper-ocean stratification, even large modification of under-ice roughness. To adequately model air–sea–ice interaction in these situations most likely requires treating small-scale exchange processes as realistically as possible.

References

Batchelor, G. K. 1970. "An Introduction to Fluid Mechanics." Cambridge Univ. Press, London.

Blackadar, A. K. & H. Tennekes. 1968. Asymptotic similarity in neutral planetary boundary layers. *J. Atmos. Sci.* **25:** 1015–1019.

Businger, J. A. & S. P. Arya. 1974. The height of the mixed layer in a stably stratified planetary boundary layer. *Adv. Geophys.* **18:** 73–92.

Deardorff, J. W. 1972. Numerical investigation of neutral and unstable planetary boundary layers. *J. Atmos. Sci.* **29:** 91–115.

Ekman, V. W. 1905. On the influence of the earth's rotation on ocean currents. *Ark. Mat., Astron. Syst.* **2:** 1–52.

———. 1906. On dead water. *In* "Scientific Results, Norwegian North Polar Expedition 1893–1896" (F. Nansen, ed.), Vol. 5, pp 1–15. Christiania, Norway.

Friehe, C. A. 1987. Review of atmospheric boundary layer research, 1983–1986. *Rev. Geophys.* **25:** 387–392.

Gill, A. E. 1982. "Atmosphere–Ocean Dynamics." Academic Press, New York.

Gordon, A. L. 1987. Mixed layer under Southern Ocean sea ice. *Eos* **68:** 1768 (abstr.).

Hachmeister, L. E. & F. A. Rigby. 1980. Laboratory studies of stratified flow interaction with topography. *In* "Proceedings of the Second International Symposium on Stratified Flows" (T. Carstens & T. McClimans, eds.), pp. 623–635. Tapir, Trondheim.

Hinze, J. O. 1975. "Turbulence." McGraw-Hill, New York.
Hunkins, K. 1966. Ekman drift currents in the Arctic Ocean. *Deep-Sea Res.* **13:** 607–620.
———. 1967. Inertial oscillations of Fletcher's Ice Island (T-3). *JGR, J. Geophys. Res.* **72:** 1165–1174.
———. 1974. An estimate of internal wave drag on pack ice. *AIDJEX Bull.* **26:** 141–152.
———. 1975. The oceanic boundary layer and stress beneath a drifting ice floe. *JGR, J. Geophys. Res.* **80:** 3425–3433.
———. 1980. Review of the AIDJEX oceanographic program. *In* "Sea Ice Processes and Models" (R. S. Pritchard, ed.), pp. 34–35. Univ. of Washington Press, Seattle.
Ikeda, M. 1986. A mixed layer beneath melting sea ice in the marginal ice zone using a one-dimensional turbulent closure model. *J. Geophys. Res.* **91:** 5054–5060.
Incropera, F. P. & D. P. DeWitt. 1985. "Fundamentals of Heat and Mass Transfer." Wiley, New York.
Johannessen, O. M. 1970. Note on some vertical profiles below ice floes in the Gulf of St. Lawrence and near the North Pole. *JGR, J. Geophys. Res.* **75:** 2857–2861.
Josberger, E. G. 1983. Sea ice melting in the marginal ice zone. *J. Geophys. Res.* **88:** 2841–2844.
———. 1987. Bottom ablation and heat transfer coefficients from the 1983 Marginal Ice Zone experiments. *J. Geophys. Res.* **92:** 7012–7016.
Langleben, M. P. 1980. Water drag coefficient at AIDJEX, station Caribou. *In* "Sea Ice Processes and Models" (R. S. Pritchard, ed.), pp. 464–471. Univ. of Washington Press, Seattle.
———. 1982. Water drag coefficient of first-year sea ice. *J. Geophys. Res.* **87:** 573–578.
Levine, M. D., C. A. Paulson & J. H. Morison. 1985. Internal waves in the Arctic Ocean: Comparison with lower-latitude observations. *J. Phys. Oceanogr.* **15:** 800–809.
Ling, C.-H. & N. Untersteiner. 1974. On the calculation of the roughness parameter of sea ice. *JGR, J. Geophys. Res.* **79:** 4112–4114.
Martinson, D. G. & C. Wamser. 1990. Ice drift and momentum exchange in winter Antarctic pack ice. *J. Geophys. Res.* (in press).
Maykut, G. A. 1985. "An Introduction to Ice in the Polar Regions," Tech. Rep. APL-UW 8510. Univ. of Washington, Seattle.
McPhee, M. G. 1974. An experimental investigation of the boundary layer under pack ice. Ph.D. Diss., Univ. of Washington, Seattle.
———. 1978. A simulation of inertial oscillation in drifting pack ice. *Dyn. Atmos. Oceans* **2:** 107–122.
———. 1979. The effect of the oceanic boundary layer on the mean drift of sea ice: Application of a simple model. *J. Phys. Oceanogr.* **9:** 388–400.
———. 1980. An analysis of pack ice drift in summer. *In* "Sea Ice Processes and Models" (R. S. Pritchard, ed.), pp. 62–75. Univ. of Washington Press, Seattle.
———. 1981. An analytic similarity theory for the planetary boundary layer stabilized by surface buoyance. *Boundary-Layer Meteorol.* **21:** 325–339.
———. 1982. "Sea Ice Drag Laws and Simple Boundary Layer Concepts, Including Application to Rapid Melting," CRREL Rep. 82-4. U.S. Army Cold Reg. Res. Eng. Lab., Hanover, New Hampshire.
———. 1983. Turbulent heat and momentum transfer in the oceanic boundary layer under melting pack ice. *J. Geophys. Res.* **88:** 2827–2835.
———. 1986a. Medium resolution turbulence clusters for upper ocean measurements under sea ice. *In* "Proceedings of the IEEE Third Working Conference on Current Measurement" (G. Appell & W. E. Woodward, eds.), pp. 163–168. Inst. Electr. Electron. Eng., New York.
———. 1986b. The upper ocean. *In* "The Geophysics of Sea Ice" (N. Untersteiner, ed.), pp. 339–394. Plenum, New York.

———. 1987. A time-dependent model for turbulent transfer in a stratified oceanic boundary layer. *J. Geophys. Res.* **92:** 6977–6986.

———. 1988. Analysis and prediction of short-term ice drift. *Trans. ASME: J Offshore Mech. Arctic Eng.* **110:** 94–100.

———. 1989. Inferring ice/ocean surface roughness from horizontal current measurements. *Trans. ASME: J. Offshore Mech. Arctic Eng.* **111:** 155–159.

McPhee, M. G. & L. H. Kantha. 1989. Generation of internal waves by sea ice. *J. Geophys. Res.* **94:** 3287–3302.

McPhee, M. G. & J. D. Smith. 1976. Measurements of the turbulent boundary layer under pack ice. *J. Phys. Oceanogr.* **6:** 696–711.

McPhee, M. G., G. A. Maykut & J. H. Morison. 1987. Dynamics and thermodynamics of the ice/upper ocean system in the marginal ice zone of the Greenland Sea. *J. Geophys. Res.* **92:** 7013–7031.

Mellor, G. & T. Yamada. 1982. Development of a turbulence closure model for geophysical fluid problems. *Rev. Geophys. Space Phys.* **20:** 851–875.

Mellor, G., M. G. McPhee & M. Steele. 1986. Ice–seawater turbulent boundary layer interaction with melting or freezing. *J. Phys. Oceanogr.* **16:** 1829–1846.

Moeng. C.-H. 1984. A large-eddy-simulation model for the study of planetary boundary-layer turbulence. *J. Atmos. Sci.* **41:** 2052–2062.

Morison, J. H. 1986. Internal waves in the Arctic Ocean: A review *In* "The Geophysics of Sea Ice" (N. Untersteiner, ed.), pp. 1163–1183. Plenum, New York.

Morison, J. H., M. G. McPhee & G. A. Maykut. 1987. Boundary layer, upper ocean, and ice observations in the Greenland Sea marginal ice zone. *J. Geophys. Res.* **92:** 6987–7011.

Muench, R. D. & L. E. Hachmeister. 1984. "Internal Wave Forces on Ice Keels in the Marginal Ice Zone: Some Preliminary Laboratory Results," CRREL Spec. Rep. 84-7, pp. 83–90. U.S. Army Cold Reg. Res. Eng. Lab., Hanover, New Hampshire.

Neshyba, S., V. T. Neal & W. Denner. 1971. Temperature and conductivity measurements under Ice Island T-3. *J. Geophys. Res.* **76:** 8107–8120.

Neumann, G. & W. J. Pierson, Jr. 1966. "Principles of Physical Oceanography." Prentice-Hall, Englewood Cliffs, New Jersey.

Obukhov, A. M. 1971. Turbulence in an atmosphere with a non-uniform temperature. *Boundary-Layer Meteorol.* **2:** 7–29.

Pease, C. H., S. A. Salo & J. E. Overland. 1983. Drag measurements for first-year sea ice over a shallow sea. *J. Geophys. Res.* **88:** 2853–2862.

Pinkel, R., S. Beck & J. H. Morison. 1986. Doppler acoustic velocity profiling in the Arctic. *In* "Proceedings of the IEEE Third Working Conference on Current Measurement" (G. Appell & W. E. Woodward, eds.), pp. 163–168. Inst. Electr. Electron. Eng., New York.

Price, J. F., E. A. Terray & R. A. Weller. 1987. Upper ocean dynamics. *Rev. Geophys.* **25:** 193–203.

Reed, R. J. & W. J. Campbell. 1962. The equilibrium drift of Ice Station Alpha. *J. Geophys. Res.* **67:** 281–297.

Rigby, F. A. 1974. Theoretical calculations of internal wave drag on sea ice. *AIDJEX Bull.* **26:** 129–140.

Shuleikin, V. V. 1938. The drift of ice-fields. *C. R. (Dokl.) Acad. Sci., URSS* **19:** 589–594.

Smith, J. D. 1974. Turbulent structure of the surface boundary layer in an ice-covered ocean. *Rapp. P.-V. Reun., Cons. Int. Explor. Mer* **167:** 53–65.

Stern, M. E. 1975. "Ocean Circulation Physics." Academic Press, New York.

Tennekes, H. & J. L. Lumley. 1972. "A First Course in Turbulence." MIT Press, Cambridge, Massachusetts.

Turner, J. S. 1973. "Buoyancy Effects in Fluids." Cambridge Univ. Press, London.

Untersteiner, N. & F. Badgley. 1965. The roughness parameters of sea ice. *J. Geophys. Res.* **70:** 4573–4577.

Villanueva, J. Z. & J. C. van Leer. 1987. Anatomy of the East Greenland Polar Front as observed by cyclesondes. *Eos* **68:** 1754 (abstr.).

Wyngaard, J. C. 1985. Structure of the planetary boundary layer and implications for its modeling. *J. Clim. Appl. Meteorol.* **24:** 1131–1142.

Wyngaard, J. C., O. R. Cote & K. S. Rao. 1974. Modeling the atmospheric boundary layer. *Adv. Geophys.* **18A:** 193–212.

Yaglom, A. M. & B. A. Kader. 1974. Heat and mass transfer between a rough wall and turbulent fluid flow at high Reynolds and Peclet numbers. *J. Fluid Mech.* **62:** 601–623.

Zilitinkevich, S. S. 1975. Resistance laws and prediction equations for the depth of the planetary boundary layer. *J. Atmos. Sci.* **32:** 741–752.